Nonlinear fluid-structure interaction problem. Part I: implicit partitioned algorithm, nonlinear stability proof and validation examples

Christophe Kassiotis, Adnan Ibrahimbegovic, Rainer Niekamp, Hermann G. Matthies

Computational Mechanics manuscript No.
(will be inserted by the editor)

Nonlinear fluid-structure interaction problem. Part I: implicit partitioned algorithm, nonlinear stability proof and validation examples.

Christophe Kassiotis · **Adnan Ibrahimbegovic** ·
Rainer Niekamp · **Hermann G. Matthies**

the date of receipt and acceptance should be inserted later

Abstract In this work we consider the fluid-structure interaction in fully nonlinear setting, where different space discretization can be used. The model problem considers finite elements for structure and finite volume for fluid. The computations for such interaction problem are performed by implicit schemes, and the partitioned algorithm separating fluid from structural iterations. The formal proof is given to find the condition for convergence of this iterative procedure in the fully nonlinear setting. Several validation examples are shown to confirm the proposed convergence criteria of partitioned algorithm. The proposed strategy provides a very suitable basics for code-coupling implementation as discussed in Part II.

Keywords fluid-structure interaction · partitioned iterations · nonlinear stability proof.

1 Introduction

Among multi-physics problems that are currently entering the mainstream of scientific research in computational mechanics (*e.g.* see [34,47]), perhaps the most frequently studied are the problems of fluid-structure interaction (*e.g.*. see [3,4,10,11,13,14,16,17,18,19,21,23,24,28,30,36,42,39,40,41,44,43,45,49,50,52,56,57,55,58,59,61] among others). The fluid-structure interaction is already an interesting problem in its own right with a vast number of important applications. However, in this work we use it as the model problem for testing the novel paradigm of solution procedure based upon the direct coupling of different codes developed for a particular sub-problem (*i.e.* either solid or fluid mechanics) into

C. Kassiotis
Saint-Venant Laboratory for Hydraulics, Université Paris-Est (Joint Research Unit EDF R&D, CETMEF, École des Ponts ParisTech), 6 quai Watier, BP 49, 78401 Chatou, France
E-mail: christophe.kassiotis@enpc.fr

A. Ibrahimbegovic
LMT-Cachan (ENS Cachan/CNRS/UPMC/PRES UniverSud Paris), 61 avenue du Président Wilson, F-94230 Cachan, France
E-mail: ai@lmt.ens-cachan.fr

R. Niekamp · H. G. Matthies
Institut für Wissenschaftliches Rechnen (TU-Braunschweig), D-38092 Braunschweig
E-mail: wire@tu-bs.de

a single code. In particular, we seek to provide the guarantees for the robustness of such a computation approach in fully nonlinear setting, where implicit schemes are used for each sub-problem, and we derive (by a formal proof) the convergence criterion for partitioned scheme iterations.

We note in passing that the current tendencies for solving fluid-structure interaction problems are mostly oriented towards the monolithic schemes, where both sub-problems are discretized in space and time in exactly the same manner resulting with a large set of (monolithic) algebraic equations to be solved simultaneously with no need to distinguish between the "fluid" and the "structure" part. To provide the unified discretization basis for monolithic approach, the most frequent choice is to use the stabilized finite elements for fluids (first proposed by Hughes and co-authors [25], and followed by [14,24,42,30,49,56, 57,54,61]), which can easily be combined with standard finite elements for nonlinear structure mechanics (*e.g.* see [7,62,33]); less frequently used possibility is to provide the finite volume scheme discretization of structure sub-problem [45] and thus provide the monolithic basis constructed by finite volume method.

We depart from these trends of using monolithic approach, and we set to develop the partitioned approach for nonlinear fluid-structure interaction. We gain in this manner the first important advantage of using standard discretization scheme that is the most suitable for a particular sub-problem. The chosen model problem will consider finite volume method for fluid and finite element method for structure. We hope in this manner to gain in our approach generality with mixing different discretization methods, as well as combining the existing codes already developed for each sub-problems.

We also note that the partitioned approach was the favorite choice of early developments (*e.g.* see [5,18,19,32]). A number of those developments were motivated by the efficiency, which was gained by treating a (large) part of the fluid-structure set of equations by explicit schemes (see [5,32]). The stability of such an approach is proved mostly for linearized stability criteria (*e.g.* see [18,19]), which still leaves the potential danger of appearance of so-called "arrested" instability (*e.g.* see [6]), where the disproportionate increase of response in the unstable regime is stopped by inelastic response of the structure that softens, but not before a non-negligible error is introduced.

We will eliminate herein any of these problems related to arrested instability by using the implicit schemes non only for each sub-problem, but also for the partitioned coupling. The resulting algorithm will thus provide the computational robustness, which will be a great interest not only for fluid-structure interaction but also for any other multi-physic problem of current interest where one would like to re-use the available codes for any particular sub-problem in a more general framework.

The main advantage of code-coupling approach for fluid-structure interaction concerns the fact that the coupling is limited only to the fluid-structure interface. Therefore, the main difficulty is reduced to enforcing the interface matching with respect to two different discretization schemes, finite element versus finite volume, as well as two different time integration schemes and different time steps. We thus split the presentation of our work in two parts, pertaining respectively, to time and to space discretization for fluid and for structure and their matching at the interface. We will deal with the interface matching for different space discretization in Part II, along with other related issues pertaining to the computational efficiency enhancements by nested parallelization. In present paper (Part I), we discuss how to accommodate any particular (implicit) scheme that ensures the unconditional stability for either fluid or structure motion computation, and how to ensure that the unconditional stability extends to partitioned solution of the fluid-structure interaction problem.

The outline of the paper is as follows. In Section 2 we give the theoretical formulation of the chosen interaction problem of the incompressible fluid and the finite deformation elastic structure. The partitioned solution algorithm for this interaction problem is presented in Section 3, and the formal proof of the stability in fully nonlinear setting in Section 4. In Section 5, we present the results of the benchmark examples and in Section 6, some closing remarks. The complementary presentation of the space discretization matching issues and nested parallel computing are discussed in Part II of this paper.

2 Theoretical formulation of fluid-structure interaction problem

We consider the interaction problem of motion of fluid (denoted further with f) and structure (denoted with s). For the sake of generality, it is supposed that theses problems are nonlinear and time dependent. This interaction is handled by the classical Direct Force-Motion Transfer (DFMT, see [18,52]) that can formally be expressed in terms of the corresponding Steklov-Poincaré operator (see [13]):

$$\begin{array}{c} \mathscr{S}_i : \mathscr{H}^{\frac{1}{2}}(\Gamma) \rightarrow \mathscr{H}^{-\frac{1}{2}}(\Gamma) \\ u_i \rightarrow \lambda_i \end{array} \quad \text{with } i \in \{f,s\} \tag{1}$$

The Steklov-Poincaré operator gives the evolution of dual field λ_i for an imposed primal field u_i on the interface space and time domain $\Gamma \times [0,T]$. In fact, this operator requires the computation of the fluid and structure problem on the complete space-time domain, governed by Navier-Stokes equations for incompressible flow and nonlinear dynamics equations for structural motion. For the problems of this kind, the Steklov-Poincaré operator is not available analytically, but rather as the results of numerical approximations. These results not only depend on the chosen model, material properties and boundary conditions, but also on discretization techniques, time integration algorithms, discrete equations solvers, etc.

The interface matching considered in the following is based on two classical mechanics principles:

(i) Continuity of primal quantities or the perfect matching condition over the interface:

$$u_s = u_f = u \qquad \text{on } \Gamma \times [0,T] \tag{2}$$

where u denotes the value of the primal variable at the interface. In the continuum setting, the time derivatives of this condition give the equivalent equations for velocity $v = \dot{u}$ and acceleration $a = \dot{v}$:

$$v_s = v_f = v; \qquad a_s = a_f = a \qquad \text{on } \Gamma \times [0,T] \tag{3}$$

However, as the result of time discretization, these conditions are no longer equivalent.

(ii) Equilibrium of dual quantities or action-reaction principle, which implies:

$$\lambda_f + \lambda_s = 0 \qquad \text{on } \Gamma \times [0,T] \tag{4}$$

The action-reaction principle in (4) can be reformulated using the Steklov-Poincaré operator defined in (1), resulting with the so-called Steklov-Poincaré formulation (see [13]):

$$\text{Find: } u \text{ on } \Gamma \times [0,T], \text{ so that: } \mathscr{S}_f(u) + \mathscr{S}_s(u) = 0 \tag{5}$$

Using the inverse of the first Steklov-Poincaré operators allows to rewrite the equilibrium of dual quantities as the following fixed-point equation that concerns only the unknown at the interface:

$$\text{Find: } u \text{ on } \Gamma \times [0,T], \text{ so that: } \; u = \mathscr{S}_s^{-1}\left(-\mathscr{S}_f(u)\right) \tag{6}$$

We note that the inverse of Steklov-Poincaré operator $\mathscr{S}^{-1}$ is no more expensive to compute than $\mathscr{S}$. The fixed-point equation can be reformulated in order to get a root equation:

$$\text{Find: } u \text{ on } \Gamma \times [0,T], \text{ so that: } \; \mathscr{S}_s^{-1}\left(-\mathscr{S}_f(u)\right) - u = 0 \tag{7}$$

where all the requested quantities are defined at the interface.

We recall that these Steklov-Poincaré operators are associated with the semi-discrete form of the continuum equations. Namely, the fluid problem is defined by an ALE formulation (*e.g.* see [12,31]) of the Navier-Stokes equations. The latter considers the fluid mesh motion that u_m is imposed by the motion of the interface u and can be written as:

$$\mathscr{R}_m(\mathbf{u}_m;\mathbf{u}) := \mathbf{K}_m\mathbf{u}_m - \mathbf{D}_m\mathbf{u} = \mathbf{0} \tag{8}$$

where $\mathbf{D}_m$ is a projection/restriction operator and $\mathbf{K}_m$ governs the extension of the boundary displacement either by a diffusion process or a pseudo-solid equation (*e.g.* see [22]). The fluid flow in this moving domain is described by the semi-discrete Navier-Stokes equations:

$$\mathscr{R}_f(\mathbf{v}_f,\mathsf{p}_f;\mathbf{u}_m) := \begin{bmatrix} \mathbf{M}_f\dot{\mathbf{v}}_f + \mathbf{N}_f(\mathbf{v}_f - \dot{\mathbf{u}}_m)\mathbf{v} + \mathbf{K}_f\mathbf{v}_f + \mathbf{B}_f\mathsf{p}_f - \mathbf{f}_f \\ \mathbf{B}_f^T\mathbf{v}_f \end{bmatrix} = \mathbf{0} \tag{9}$$

where $\mathbf{v}_f$, $\dot{\mathbf{v}}_f$ and p_f are fluid velocity, its derivative and fluid pressure $\mathbf{M}_f$ is a (positive definite) mass matrix, $\mathbf{N}_f$ is a (non-symmetric) advection matrix, $\mathbf{K}_f$ is the matrix with diffusion terms, $\mathbf{B}_f$ stands for the gradient matrix, and $\mathbf{f}_f$ is the driving force on the flow. The discretization process leading to fluid equations of motion and incompressibility constraint in (9) is carried out by Finite Volume Method [22].

The Finite Element Method [63] is used for the structure sub-problem, resulting with structural semi-discrete equations of motion:

$$\mathscr{R}_s(\mathbf{u}_s;\lambda) := \mathbf{M}_s\ddot{\mathbf{u}}_s + \mathbf{f}_s^{\text{int}}(\mathbf{u}_s) - \mathbf{f}_s^{\text{ext}}(\lambda) = \mathbf{0} \tag{10}$$

where $\mathbf{M}_s$ is the mass matrix, $\mathbf{f}_s^{\text{int}}$ is the internal force which is highly non-linear if large deformation or complex material behavior is used (*e.g.*. [33]), and $\mathbf{f}_s^{\text{ext}}$ is the external force vector.

Algorithm 1 Steklov-Poincaré operator for fluid: $\mathscr{S}_f$

Require: Fluid state variable at time T_N

1: Impose displacement of mesh at fluid-structure interface:
$u_m = u$ on $\Gamma \times [T_N, T_{N+1}]$
2: Solve mesh intern nodes displacement:
$\mathscr{R}_m(u_m;u) = 0$ on $\Omega_f \times [T_N, T_{N+1}]$
3: Solve fluid problem in ALE formulation:
$\mathscr{R}_f(v_f, p_f; u_f) = 0$ on $\Omega_f \times [T_N, T_{N+1}]$
4: Get boundary traction force at the interface:
$\lambda = -\sigma_f n$ on $\Gamma \times [T_N, T_{N+1}]$

With this notation on hand we can provide the explicit form of the Steklov-Poincaré operator for fluid and for structure, which can be expressed in terms of **Algorithm 1** and **2**.

Algorithm 2 Poincaré-Steklov operator for structure: $\mathscr{S}_s^{-1}$

Require: Solid state variable at time T_N
1: Impose boundary traction force at fluid-structure interface:
$\sigma_s n = \lambda$ on $\Gamma \times [T_N, T_{N+1}]$
2: Solve structure problem:
$\mathscr{R}_s(u_s; \lambda) = 0$ on $\Omega_s \times [T_N, T_{N+1}]$
3: Get boundary displacement at the interface:
$u = u_s$ on $\Gamma \times [T_N, T_{N+1}]$

3 Discrete force motion transfer (DFMT) – Explicit versus implicit scheme for interface matching

We assume in the subsequently that each sub-problem (either fluid flow or structural motion) has been integrated by an implicit time-stepping scheme (wide variety is available in [22, 33]). We are thus only left with integrating the interface matching unknowns.

Each of Steklov-Poincaré operators involves the complete domain for either fluid and solid, and furthermore, each results in a set of nonlinear equations to be solved. Therefore, an iterative scheme has to be defined to compute the solution of the coupled problem. To that end, one can use any of the formulation in (5), (6) or (7) and corresponding iterative schemes, such as: i) the one in (6) with Picard like iterative schemes [59,41]; ii) the one in (7) with Newton [44,21] or quasi-Newton [26,56,11] iterations; iii) the one in (5) with non-linear Richardson strategy [13,20].

3.1 Generalized Conventional Serial Staggered (GCSS) algorithm

This explicit approach, yet called *weak* coupling, tries to provide the best possible approximation of the interface matching solving only once Steklov-Poincaré operator for each sub-problem and in each time step. More precisely, we consider the evolution of the fluid-structure interaction problem in a time-interval (or *window*) $[T_N, T_{N+1}]$ of size Δt. The idea is to solve at each time step a single Picard-iteration of the fixed-point equation in (6):

$$u_{N+1} = \mathscr{S}_s^{-1}\left(-\mathscr{S}_f\left(u_N\right)\right) \tag{11}$$

However, this leads to bad conservation properties at the interface, which can be improved by the addition of a better predictor $\mathscr{P}$. This results with the **Algorithm 3**.

Algorithm 3 Generalized Conventional Serial Staggered

1: Given: initial time $T = T_0$, final time $T_{\max}$, window size Δt, initial interface displacement u_0.
2: **while** $T < T_{\max}$ **do**
3: Predict displacement: $u_{N+1}^{\mathscr{P}} = \mathscr{P}(u_N, \dot{u}_N, u_{N-1}, \dots)$
4: Solve problem f: $\lambda_{N+1} = \mathscr{S}_f(u_{N+1}^{\mathscr{P}})$
5: Solve problem s: $u_{N+1} = \mathscr{S}_s(\lambda_{N+1})$
6: $N \leftarrow N+1$ and $T \leftarrow T + \Delta t$
7: **end while**

Note that we do not impose the way the time integration is performed, but only that the fluid and the structure part be collocated at the end of the same time windows. When considering equal time step size for fluid and structure, this Direct Force-Motion Transfer

algorithm is named Conventional Serial Staggered (DFMT-CSS) (see [17,18]). We can also consider the so-called Sub-cycled Conventional Staggered Scheme (DFMT-SCSS) where time steps selected for integration of fluid flow and structure motion are not the same size. Usually, the characteristic time scale of the fluid is smaller, and thus we consider integration for the fluid part with many small time steps on the window $[T_N, T_{N+1}]$.

The interface displacements for the structure at time T_{N+1} is therefore u_{N+1} while for the fluid, the final value is set by the predictor as a function of u_N. For that reason, the interface matching condition at T_{N+1}, cannot be fulfilled by this explicit scheme and we obtain:

$$u_{s,N+1} = u_{N+1} \neq u_{f,N+1} = u^{\mathscr{P}}_{N+1} \tag{12}$$

Moreover there is no reason that the interface matching condition be fulfilled for the velocity. As a result, an energy error is introduced by this kind of exchange at the interface which can be estimated by computing the energy transfer to the interface for both fluid and structure [50,16].

The first analysis of this explicit DFMT partitioned strategy [19] printed out the upper limit on the time step size beyond which each numerical simulation of structure motion explicitly coupled to fluid flow diverges. This upper limit depends on the fluid/structure density ratio and on the speed of sound in the fluid medium. This criterion directly applied to incompressible flows with infinite wave speed, predicts immediate instability for any chosen time step. The instability phenomenon are noticed in [59,24,41,46]. and a simplified model is proposed [10] for their prediction. The instability of explicit interface matching is clearly shown by the numerical examples in Sec. 5.

3.2 Direct Force-Motion Transfer Block Gauss–Seidel (DFMT-BGS) algorithm for implicit matching

By enforcing the continuity of primal variables at the interface we can eliminate the energy errors that characterize the explicit interface matching. This ought to be done by iterating on the following residual to reduce its value below the chosen tolerance:

$$r_{N+1} := u_{s,N+1} - u_{f,N+1} \simeq 0 \quad \leq \texttt{TOL} \tag{13}$$

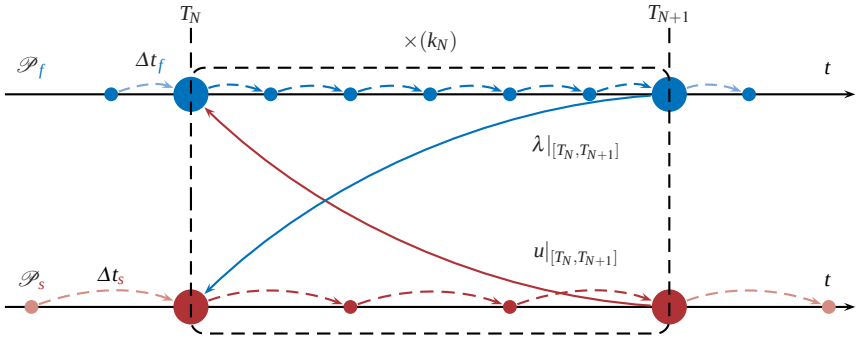

Fig. 1 Block Gauß-Seidel coupling algorithm for fluid $(\mathscr{P}_f)$ structure $(\mathscr{P}_s)$ interaction problems; this iterative scheme is applied (k_N) times until convergence on a window $[T_N, T_{N+1}]$.

In this way we obtain an implicit algorithm requiring more than one iteration to enforce the interface matching condition. The chosen order of iterations, as presented in Fig. 1, corresponds to the Block-Gauß-Seidel algorithm for fluid-structure interaction problem. We also show in Fig. 1 that not only the value at synchronization points T_n or T_{n+1}, but also the interpolated evolution of variables have to be exchanged in the entire time-interval $t \in [T_n, T_{n+1}]$.

Contrary to explicit algorithms which generate spurious energy at the interface, the present implicit interface matching algorithm enforce the same evolution of the primal variables at the fluid-structure interface. In other words, an iterative solution for equation (6) is performed by using the Picard iteration:

$$u_{N+1}^{(k+1)} = \mathscr{G}\left(u_{N+1}^{(k)}\right); \qquad \mathscr{G} = \mathscr{S}_s^{-1} \circ -\mathscr{S}_f \tag{14}$$

where $\mathscr{S}_f$ and $\mathscr{S}_s$ are Steklov-Poincaré operators for fluid and structure defined previously. The Picard iterations will continue until convergence of interface residual is achieved:

$$r_{N+1}^{(k)} = u_{s,N+1}^{(k)} - u_{f,N+1}^{(k)} = \mathscr{G}\left(u_{N+1}^{(k)}\right) - u_{N+1}^{(k)} \tag{15}$$

Such a Block-Gauß-Seidel algorithm with implicit interface matching, further denoted as DFTM-BGS, can be presented as a natural generalization of the explicit algorithms. We can thus write:

Algorithm 4 Direct Force-Motion Transfer Block-Gauß-Seidel

1: Given: initial time $T = T_0$, final time $T_{\max}$, window size Δt, initial interface displacement u_0.
2: **while** $T < T_{\max}$ **do**
3: $(k) = 0$
4: Predict displacement: $u_{N+1}^{(0)} = \mathscr{P}(u_N^{(k_{\max})}, \dot{u}_N^{(k_{\max})}, u_{N-1}^{(k_{\max})}, \dots)$
5: **repeat**
6: Perform Picard iteration: $\mathscr{G}\left(u_{N+1}^{(k)}\right)$
7: Compute residual: $r_{N+1}^{(k)} = \mathscr{G}\left(u_{N+1}^{(k)}\right) - u_{N+1}^{(k)}$
8: Update interface primal variable: $u_{N+1}^{(k+1)} = u_{N+1}^{(k)} + r_{N+1}^{(k)}$
9: **do** $(k) \leftarrow (k) + 1$
10: **until** $\|r_N^{(k-1)}\| \geq \texttt{TOL}$
11: $N \leftarrow N + 1$ and $T \leftarrow T + \Delta t$
12: **end while**

As illustrated in Figure 2, this fixed-point algorithm based on Picard iterations for the time has the main drawback that the search directions for u and λ variables do not exploit any information from the fixed-point function $\mathscr{G}$ nor the Steklov-Poincaré operators $\mathscr{S}_f$ and $\mathscr{S}_s$. Therefore, quite a few iterations may be needed to reach the convergence.

In order to improve the convergence of the DFMT-BGS method, we can use a more accurate update:

$$u_{N+1}^{(k+1)} = u_{N+1}^{(k)} + \mathscr{H}\, r_{N+1}^{(k)} \tag{16}$$

The choice of matrix $\mathscr{H}$ above should be made to improve the method convergence. Our favorite choice for constructing $\mathscr{H}$ is using a secant methods which can keep the cost of each iteration as low as possible. In particular, an approximation of $\mathscr{H}$ by a scalar ω employed herein with optimal value at each iteration $\omega^{(k)}$ obtained by Aitken's relaxation. For such a choice the convergence rate is able to reach $\alpha \simeq 1.6$.

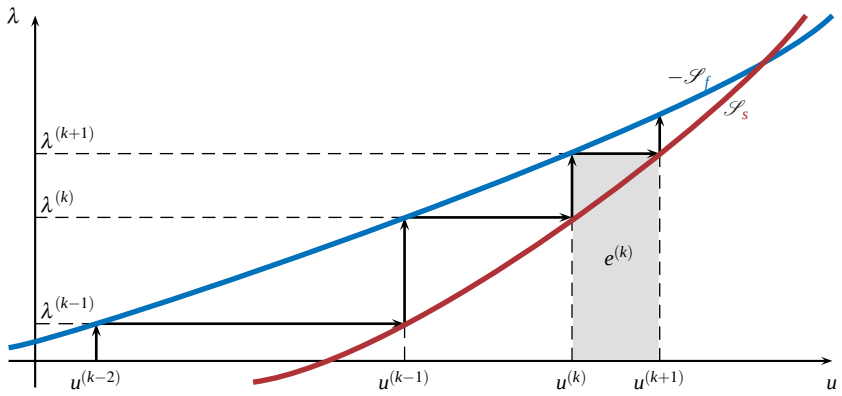

Fig. 2 Implicit for interface matching by non-linear Block Gauß-Seidel.

We note in passing that various other improvements for constructing $\mathscr{H}$ matrix have been attempted (*e.g.* see [40,43,59,11]), but we did not find them indispensable for the studies presented herein where dynamic Aitken relaxation proved to be sufficient. Moreover, for such a choice we are able to provide the formal proof of stability of DFMT-BGS in fully nonlinear framework.

4 Proof of stability and convergence of DFMT-BGS

4.1 Reformulation of the fluid-structure interaction problem in a Differential Algebraic Equation framework

The main goal of this section is to confirm the stability of the partitioned approach for coupled fluid-structure interaction problems with implicit interface matching based upon the DFMT-BGS iterative scheme. At the outset, we assume that the approximate choice of stable and accurate integration schemes is made to solve for fluid flow and structure motion[1]. We can thus focus only upon the interface matching computations. To that end, we will first recast the DFMT-BGS algorithm formulated in the general framework of *differential-algebraic equations* (DAE). This allows to follow in the footsteps of the proof of nonlinear stability of the partitioned algorithm provided in [2].

The first sub-problem pertaining to the fluid flow on a moving domain, discretized by Finite Volume Method, is defined jointly by equations (8) and (9), which can be written as:

$$\begin{aligned} 0 &= r_f(x_f(t), x_s(t), y_f(t), \lambda(t)) \\ &= \begin{bmatrix} \mathbf{K}_m \mathbf{u}_m - \mathbf{D}_m \mathbf{u}_s \\ \mathbf{M}_f \dot{\mathbf{v}}_f + \mathbf{N}_f(\mathbf{v}_f - \dot{\mathbf{u}}_m)\mathbf{v} + \mathbf{K}_f \mathbf{v}_f + \mathbf{B}_f \mathsf{p}_f - \mathbf{f}_f - \mathbf{D}_f^T \lambda \\ \mathbf{B}_f^T \mathbf{v}_f \end{bmatrix} \end{aligned} \tag{17}$$

In (17) above $\mathbf{v}_f$ is fluid velocities, and $\mathbf{u}_m$ is the mesh displacements, which are gathered together in $x_f = (\mathbf{v}_f, \mathbf{u}_m)$, while their time derivatives as well as the pressure field are placed

[1] It is also assumed that fluid flow and structure motion are computed by the corresponding software products, to be coupled for solving a fluid-structure interaction problem; the details of software coupling are discussed in Part II of this paper.

in $y_f = (\dot{\mathbf{v}}_f, \mathsf{p}, \dot{\mathbf{u}}_m)$. The forces at the interface are denoted with λ and matrix $\mathbf{D}_f$ is the result of their interpolation across the interface from the fluid side. The residual r_f gathers the mesh motion for ALE, the coupled discretized momentum equation and incompressibility condition. Rewriting the incompressibility condition using the acceleration in order to reduce the order of the DAE associated with incompressible fluid problem leads to:

$$\begin{aligned} 0 &= r_f(x_f(t), x_s(t), y_f(t), \lambda(t)) \\ &= \begin{bmatrix} \mathbf{K}_m \dot{\mathbf{u}}_m - \mathbf{D}_m \dot{\mathbf{u}}_s \\ \mathbf{M}_f \dot{\mathbf{v}}_f + \mathbf{N}_f(\mathbf{v}_f - \dot{\mathbf{u}}_m)\mathbf{v} + \mathbf{K}_f \mathbf{v}_f + \mathbf{B}_f \mathsf{p}_f - \mathbf{f}_f - \mathbf{D}_f^T \lambda \\ -\mathbf{B}_f^T \mathbf{M}_f^{-1} \left(\mathbf{N}_f(\mathbf{v}_f - \dot{\mathbf{u}}_m)\mathbf{v} + \mathbf{K}_f \mathbf{v}_f + \mathbf{B}_f \mathsf{p}_f - \mathbf{f}_f - \mathbf{D}_f^T \lambda \right) \end{bmatrix} \end{aligned} \tag{18}$$

Considering now the structure motion, we will gather the primal variables, the solid displacements $\mathbf{u}_s$ and velocities $\dot{\mathbf{u}}_s$, in the same vector $x_s = (\mathbf{u}_s, \dot{\mathbf{u}}_s)$, whereas the acceleration is denoted as $y_s = \ddot{\mathbf{u}}_s$. The residual form of the equation of motion can then be written:

$$0 = r_s(x_s(t), x_f(t), y_s(t), \lambda(t)) \tag{19}$$

The last equation can be written explicitely as:

$$r_s(x_s(t), x_f(t), y_s(t), \lambda(t)) := \left[\mathbf{M}_s \ddot{\mathbf{u}}_s + \mathbf{f}_s^{\text{int}}(\mathbf{u}_s) - \mathbf{f}_s^{\text{ext}} - \mathbf{D}_s^T \lambda \right] \tag{20}$$

where the $\mathbf{D}_s$ indicates the force distribution at the interface on the structure side.

The interface matching equation, which accounts for interaction, can be stated in terms of acceleration:

$$0 = r_\lambda(x_f(t), x_s(t), y_f(t), y_s(t)) := -\mathbf{D}_s \ddot{\mathbf{u}}_s + \mathbf{D}_f \dot{\mathbf{v}}_f \tag{21}$$

With this notation in hand, the proposed DFMT-BGS algorithm with implicit interface matching can be stated as follows: first solve the fluid sub-problem together with the continuity equation at the interface:

$$\begin{aligned} \partial_t {x_f}^{(k)} &= f_{r_f}({x_f}^{(k)}, {x_s}^{(k-1)}, {y_f}^{(k)}) \\ 0 &= r_f({x_f}^{(k)}, {x_s}^{(k-1)}, {y_f}^{(k)}, \lambda^{(k)}) \\ 0 &= r_\lambda({x_f}^{(k)}, {x_s}^{(k-1)}, {y_f}^{(k)}, {y_s}^{(k-1)}) \end{aligned} \tag{22}$$

and then solve the structure sub-problem with imposed forces at the interface:

$$\begin{aligned} \partial_t {x_s}^{(k)} &= f_{r_s}({x_f}^{(k)}, {x_s}^{(k)}, {y_s}^{(k)}) \\ 0 &= r_s({x_f}^{(k)}, {x_s}^{(k)}, {y_s}^{(k)}, \lambda^{(k)}) \end{aligned} \tag{23}$$

4.2 Error propagation, stability and convergence of DFMT-BGS algorithm

In the examples to follow we solved each nonlinear sub-problem by a dedicated solver (*e.g.* conserving algorithm for the structure (see for instance [35]), *segregated approach* like PISO for the fluid part [22]). The final stability results is valid in a more general context as long as sub-problem computation remains stable and convergent. Thus we only need to confirm the convergence of the iterative DFMT-BGS procedure for the interface matching.

We introduce the following notations: the subscript N for the restriction of the function of time t to the interval $[T_{N-1}, T_N]$, $h = T_N - T_{N-1}$, the superscripts (k) for the iteration counter of the DFMT-BGS for interface matching procedure and the Δ symbol denoting

the distance of numerical approximation to the exact solution, $\Delta x_N^{(k)} = x_N^{(k)} - x^\star$. Moreover, the same time steps for each sub-problem of the fluid-structure interaction are not needed; for instance the fluid problem can be solved with many smaller time steps as opposed to a single time step for structure. The time interpolation of the evolution on the window has to be considered *a priori*.

The stability of DFMT-BGS operator split procedures is mainly governed by error propagation from one window, say N, to the following $N+1$. In [2], a stability study of the partitioned approach for differential-algebraic systems of equations (DAE) that characterize the multi-body system dynamics is given. The stability proof given in [2] considers the case Lagrange multipliers or dual, rather than primal variable values are exchanged at the interface from one iteration to the next. In [1], the stability criterion corresponding to the block-Gauß-Seidel algorithm such as the one used herein is given [44], but without any proof. In the following a detailed proof for DFMT-BGS algorithm that cannot be found in the literature for the fluid-structure interaction context is given.

We note in passing that the same kind of results can be used for other coupled problems where the time integration schemes of the sub-problems are different, such as thermomechanics [37] or with different time scales for mechanics and thermal component as well as a generalized non-linear operator split for problems with internal variables [38]. However, the proof given herein is entirely original, as the dual quantities are exchanged in each iteration.

The main result can be stated as follows:

Theorem 1 *There exists $C \in \mathbb{R}_+$ such that for all $(k) > 1$*

$$\max_n \left(\|\Delta x_{f_n}^{(k)}\| + \|\Delta x_{s_n}^{(k)}\| + \|\Delta y_{f_n}^{(k)}\| + \|\Delta y_{s_n}^{(k)}\| + \|\Delta \lambda_n^{(k)}\| \right) < C \cdot \max_n \left(\mu^{k-2} \left(\|\Delta x_{f_n}^{(0)}\| + \|\Delta x_{s_n}^{(0)}\| \right) + \mu^{k-1} \|\Delta y_{s_n}^{(0)}\| \right)$$

where: $\mu = \alpha + \mathscr{O}(H)$ and α the contraction constant characterizing the operator split procedure employed to solve this nonlinear interaction problems, which can be written as:

$$\alpha = \max_n \left\| \left[\partial_{y_s} r_\lambda \left[\partial_{y_s} r_s \right]^{-1} \partial_\lambda r_s \right]^{-1} \partial_{y_f} r_\lambda \left[\partial_{y_f} r_f \right]^{-1} \partial_\lambda r_f \right\|$$

The main condition on contraction property with $\alpha < 1$ will guarantee the convergence of the operator split procedure for the given time window when $(k) \longrightarrow \infty$. We set now to apply this stability criterion to the DFMT-BGS for fluid-structure interaction presented in the previous section. We thus obtain:

(i) Fluid sub-problem on a moving domain discretized with FV method:

$$\partial_{y_f} r_f = \begin{bmatrix} \mathbf{K}_m & \mathbf{0} & \mathbf{0} \\ \partial_{\dot{\mathbf{u}}_m} (\mathbf{N}_f (\mathbf{v}_f - \dot{\mathbf{u}}_m) \mathbf{v}) & \mathbf{M}_f & \mathbf{B}_f \\ -\mathbf{B}_f^T \mathbf{M}_f^{-1} \partial_{\dot{\mathbf{u}}_m} (\mathbf{N}_f (\mathbf{v}_f - \dot{\mathbf{u}}_m) \mathbf{v}) & \mathbf{0} & -\mathbf{B}_f^T \mathbf{M}_f^{-1} \mathbf{B}_f \end{bmatrix} \tag{24}$$

and

$$\partial_\lambda r_f = \begin{bmatrix} \mathbf{0} \\ -\mathbf{D}_f^T \\ \mathbf{B}_f^T \mathbf{M}_f^{-1} \mathbf{D}_f^T \end{bmatrix} \tag{25}$$

(ii) Matching condition that corresponds to the continuity at the interface:

$$\partial_{y_s} r_\lambda = -\mathbf{D}_s; \; \partial_{y_f} r_\lambda = \begin{bmatrix} \mathbf{0} & \mathbf{D}_f & \mathbf{0} \end{bmatrix} \tag{26}$$

(iii) Structural problem solved with a FE method:

$$\partial_{y_s} r_s = \mathbf{M}_s;\ \partial_\lambda r_s = -\mathbf{D}_s^T \tag{27}$$

Combining the given corresponding values of Jacobian computed for all these equations leads to the corresponding value of the contraction constant α for fluid-structure interaction, that can be written after simplification:

$$\alpha = \max_n \left\| \left[\partial_{y_s} r_s\right]^{-1} \partial_\lambda r_s \left[\partial_{y_f} r_\lambda \ \left[\partial_{y_f} r_f\right]^{-1} \partial_\lambda r_f\right]^{-1} \partial_{y_s} r_\lambda \right\| =$$
$$\max_n \left\| \mathbf{M}_s^{-1}\mathbf{D}_s^T \left[\mathbf{D}_f \mathbf{M}_f^{-1} \left(\mathbf{1} + \mathbf{B}_f \left(\mathbf{B}_f^T \mathbf{M}_f^{-1} \mathbf{B}_f\right)^{-1} \mathbf{B}_f^T \mathbf{M}_f^{-1}\right) \mathbf{D}_f^T\right]^{-1} \mathbf{D}_s \right\|$$

This criterion shows that the numerical computation is highly linked to the material properties and more generally to the model chosen for the fluid and the structure sub-problems. As the first approximation an estimate for α can be provided by the mass ratio between the fluid $\mathbf{M}_f$ and the solid part $\mathbf{M}_s$ weighted by some geometrical conditions for the field transfer defined in $\mathbf{D}_f$ and $\mathbf{D}_s$. When the mass ratio increase, the scheme can become unstable. The terms in $\mathbf{B}_f$ show the influence of the incompressibility condition, resulting in the stability domain reductionand through the added-mass effect (see [24,23,41]). In order to the domain of stability for iterative DFMT-BGS procedure, Aitken's relaxation can be used as presented in the previous section. The stability of such modified algorithm can then be proved following the recepies from [2] for pre-conditioned algorithm. This proof will not be given herein, but only the corresponding improvement shown in the numerical examples.

4.3 Proofs for stable error propagation

The proof of the stability error propagation theorem is given as follows:

(i) The error bound for one iteration of the operator split procedure for an approximation in the neighborhood of the solution is given in **Lemma 1**.
(ii) In **Lemma 2**, a recursive application of **Lemma 1** gives a bound for (k) iteration of the operator split procedure.
(iii) The proof is concluded by the application of the two Lemmas with suitable arguments.

Lemma 1 *Consider $\mathscr{U}_{\gamma_0}$ a neighborhood of the solution $\left(x_f{}^\star, x_s{}^\star, y_s{}^\star\right)$:*

$$\mathscr{U}_{\gamma_0} = \left\{ \left(x_f, x_s, y_s\right) \,\middle|\, \left\|x_f - x_f{}^\star\right\| + \left\|x_s - x_s{}^\star\right\| + \left\|y_s - y_s{}^\star\right\| \leqslant \gamma_0 \right\}$$

There exists $(C, H_0, \gamma_0) \in \mathbb{R}_+^3$ such that:

$$\forall \left(\left(x_f{}^{(0)}, x_s{}^{(0)}, y_s{}^{(0)}\right), \left(\tilde{x_f}{}^{(0)}, \tilde{y_s}{}^{(0)}, \tilde{\lambda}^{(0)}\right) \right) \in \mathscr{U}_{\gamma_0}{}^2, \quad \forall H < H_0,$$

$$\begin{bmatrix} \|\delta x_f{}^{(1)}\| \\ \|\delta x_s{}^{(1)}\| \\ \|\delta y_s{}^{(1)}\| \end{bmatrix} \leqslant \begin{bmatrix} CH & CH & CH \\ CH & CH & CH \\ C & C & \hat{\alpha} + CH \end{bmatrix} \begin{bmatrix} \|\delta x_f{}^{(0)}\| \\ \|\delta x_s{}^{(0)}\| \\ \|\delta y_s{}^{(0)}\| \end{bmatrix} + \begin{bmatrix} \|\delta x_f{}^{(0)}(T_n)\| \\ \|\delta x_s{}^{(0)}(T_n)\| \\ 0 \end{bmatrix}$$

with δ denoting the distance between two approximations, i.e. $\delta x^{(k)} = x^{(k)} - \tilde{x}^{(k)}$ and

$$\hat{\alpha} = \alpha + \mathscr{O}(1) \left(\|\Delta x_f{}^{(0)}\| + \|\Delta x_s{}^{(0)}\| + \|\Delta x_s{}^{(0)}\| + \|\Delta \tilde{x_f}{}^{(0)}\| + \|\Delta \tilde{x_s}{}^{(0)}\| + \|\Delta \tilde{x_s}{}^{(0)}\| \right)$$

Proof (of Lemma 1) By inserting $(x_f{}^{(0)}, x_s{}^{(0)}, y_s{}^{(0)}) \in \mathscr{U}_{\gamma_0}$ in the proposed algorithm, we obtain the evolution equation of the fluid sub-problem (22) as the first step of the staggered scheme:

$$\left\{\begin{array}{rl} \partial_t x_f{}^{(1)} &= f_{r_f}(x_f{}^{(1)}, x_s{}^{(0)}, y_f{}^{(1)}) \\ 0 &= r_f(x_f{}^{(1)}, x_s{}^{(0)}, y_f{}^{(1)}, \lambda^{(1)}) \\ 0 &= r_\lambda(x_f{}^{(1)}, x_s{}^{(0)}, y_f{}^{(1)}, y_s{}^{(0)}) \end{array}\right. \qquad \text{with } x_f{}^{(1)}(T_N) = x_f{}^{(0)}(T_N) \tag{28}$$

For the second sub-system in (23), the evolution of the structure sub-problem under the loading $\lambda^{(k)}$ is recovered:

$$\left\{\begin{array}{rl} \partial_t x_s{}^{(1)} &= f_{r_s}(x_f{}^{(1)}, x_s{}^{(1)}, y_s{}^{(1)}) \\ 0 &= r_s(x_f{}^{(1)}, x_s{}^{(1)}, y_s{}^{(1)}, \lambda^{(1)}) \end{array}\right. \qquad \text{with } x_s{}^{(1)}(T_N) = x_s{}^{(0)}(T_N) \tag{29}$$

The same kind of evolution is found for any other initial value in the neighborhood of the solution: $(\tilde{x_f}{}^{(0)}, \tilde{x_s}{}^{(0)}, \tilde{y_s}{}^{(0)}) \in \mathscr{U}_{\gamma_0}$.

With a regularity assumption which guarantees that f_{r_f} and f_{r_s} satisfy Lipschitz conditions w.r.t. to their arguments (x_f, x_s, y_f, y_s),[2], we can obtain the following bound after one time integration over the window $N+1$ for $\delta x_f{}^{(1)} = x_f{}^{(1)} - \tilde{x_f}{}^{(1)}$ and $\delta x_s{}^{(1)} = x_s{}^{(1)} - \tilde{x_s}{}^{(1)}$:

$$\left\{\begin{array}{l} \|\delta x_f{}^{(1)}\| \leqslant \|\delta x_f{}^{(0)}(T_N)\| + \mathscr{O}(H)(\|\delta x_f{}^{(0)}\| + \|\delta y_f{}^{(1)}\|) \\ \|\delta x_s{}^{(1)}\| \leqslant \|\delta x_s{}^{(0)}(T_N)\| + \mathscr{O}(H)(\|\delta x_s{}^{(0)}\| + \|\delta y_s{}^{(1)}\|) \end{array}\right. \tag{30}$$

Our goal is now to provide a bound to the difference in the primal unknown that will be imposed at the next iteration $\|\delta y_s{}^{(1)}\|$. For a fixed time t, the algebraic equations are summarized to $F(0) = F(1) = 0$ with:

$$F(\theta) = \begin{bmatrix} r_f(x_f{}^{(1),\theta}, x_s{}^{(0),\theta}, y_f{}^{(1),\theta}, \lambda^{(1),\theta}) \\ r_\lambda(x_f{}^{(1),\theta}, x_s{}^{(0),\theta}, y_f{}^{(1),\theta}, y_s{}^{(0),\theta}) \\ r_s(x_f{}^{(1),\theta}, x_s{}^{(1),\theta}, y_s{}^{(1),\theta}, \lambda^{(1),\theta}) \end{bmatrix}, \quad \theta \in \{0,1\} \tag{31}$$

where x^θ can be written as $x^\theta = (1-\theta)x + \theta\tilde{x}$.

The identity $F(1) - F(0) = \int_0^1 F'(\theta)\,\mathrm{d}\theta = 0$ further gives:

$$\overbrace{\int_0^1 \left(\begin{bmatrix} \partial_{y_f} r_f & \partial_\lambda r_f & 0 \\ \partial_{y_f} r_\lambda & 0 & 0 \\ 0 & \partial_\lambda r_s & \partial_{y_s} r_s \end{bmatrix} \begin{bmatrix} \delta y_f{}^{(1)} \\ \delta\lambda^{(1)} \\ \delta y_s{}^{(1)} \end{bmatrix} + \begin{bmatrix} 0 \\ \partial_{y_s} r_\lambda \\ 0 \end{bmatrix} \delta y_s{}^{(0)} \right) \mathrm{d}\theta}^{\text{independent of } \theta}$$

$$+ \mathscr{O}(1)\left(\|\delta x_s{}^{(0)}\| + \|\delta x_f{}^{(1)}\| + \|\delta x_s{}^{(1)}\| \right) = 0$$

In the equation above the arguments $x_f{}^{(1)}$ and $x_s{}^{(1)}$ of the Jacobian that are placed in the neighborhood $\mathscr{U}_{\gamma_0}$ of size $\mathscr{O}(\gamma_0)$ of the solution $(x_f{}^\star, x_s{}^\star)$ are neglected. If γ_0 is sufficiently

[2] Regarding this regularity assumption, see the remark at the end of this proof.

small, then we can easily solve the previous equation, provided the algebraic equations give a non-singular matrix[3].

$$
\begin{aligned}
&- \begin{bmatrix} \partial_{y_f} r_f & \partial_\lambda r_f & 0 \\ \partial_{y_f} r_\lambda & 0 & 0 \\ 0 & \partial_\lambda r_s & \partial_{y_s} r_s \end{bmatrix}^{-1} \begin{bmatrix} 0 \\ \partial_{y_s} r_\lambda \\ 0 \end{bmatrix} \\
&= \begin{bmatrix} & \\ \hline & \\ \hline & \\ \left[\partial_{y_s} r_s\right]^{-1} \partial_\lambda r_s & \left[\partial_{y_f} r_\lambda \left[\partial_{y_f} r_f\right]^{-1} \partial_\lambda r_f\right]^{-1} \partial_{y_s} r_\lambda \end{bmatrix}
\end{aligned}
\tag{32}
$$

thus the contractivity coefficient α can be defined as:

$$
\alpha = \max_n \left\| \left[\partial_{y_s} r_s\right]^{-1} \partial_\lambda r_s \left[\partial_{y_f} r_\lambda \left[\partial_{y_f} r_f\right]^{-1} \partial_\lambda r_f\right]^{-1} \partial_{y_s} r_\lambda \right\|
$$

Using this inverse calculation in (32) gives the following bounds for the difference between the two coupled problems after one iteration:

$$
\begin{aligned}
\|\delta {y_f}^{(1)}\| &\leqslant \mathscr{O}(1)\Big(\|\delta {x_f}^{(0)}\| + \|\delta {x_s}^{(0)}\| + \|\delta {y_s}^{(0)}\| + \|\delta {x_f}^{(1)}\| + \|\delta {x_s}^{(1)}\|\Big) \\
\|\delta {y_s}^{(1)}\| &\leqslant \hat{\alpha}\|\delta {y_s}^{(0)}\| + \mathscr{O}(1)\Big(\|\delta {x_f}^{(0)}\| + \|\delta {x_s}^{(0)}\| + \|\delta {x_f}^{(1)}\| + \|\delta {x_s}^{(1)}\|\Big)
\end{aligned}
$$

where:

$$
\hat{\alpha} = \alpha + \mathscr{O}(1)\Big(\|\Delta {x_f}^{(0)}\| + \|\Delta {x_s}^{(0)}\| + \|\Delta \lambda^{(0)}\| + \|\Delta \tilde{x_f}^{(0)}\| + \|\Delta \tilde{x_s}^{(0)}\| + \|\Delta \tilde{\lambda}^{(0)}\|\Big)
$$

Inserting the inequality above in the Lipschitz condition in (30) gives:

$$
\begin{aligned}
\|\delta {x_f}^{(1)}\| &\leqslant \mathscr{O}(H)\left(\|\delta {x_f}^{(0)}\| + \|\delta {x_s}^{(0)}\| + \|\delta {y_s}^{(0)}\|\right) + \|\delta {x_f}^{(0)}(T_N)\| \\
\|\delta {x_s}^{(1)}\| &\leqslant \mathscr{O}(H)\left(\|\delta {x_f}^{(0)}\| + \|\delta {x_s}^{(0)}\| + \|\delta {y_s}^{(0)}\|\right) + \|\delta {x_s}^{(0)}(T_N)\| \\
\|\delta {y_s}^{(1)}\| &\leqslant (\hat{\alpha} + \mathscr{O}(H))\,\|\delta {y_f}^{(0)}\| + \mathscr{O}(1)\left(\|\delta {x_f}^{(0)}\| + \|\delta {x_s}^{(0)}\|\right)
\end{aligned}
$$

Rewriting the equation above in matrix form completes the proof of **Lemma 1**.

Lemma 2 *Provided that the assumptions of the previous Lemma are satisfied and assume that* $\hat{\alpha} < 1$ *and* $C > \hat{\alpha}$*, one can write:*

$$
\exists \hat{C} \in \mathbb{R}_+ \qquad \textit{such that} \qquad \forall k > 1, \forall H \leqslant H_0
$$

$$
\begin{bmatrix} \|\delta {x_f}^{(k)}\| \\ \|\delta {x_s}^{(k)}\| \\ \|\delta {y_s}^{(k)}\| \end{bmatrix} \leqslant \begin{bmatrix} 1 + \hat{C}H\|\delta {x_f}^{(0)}(T_N)\| \\ 1 + \hat{C}H\|\delta {x_s}^{(0)}(T_N)\| \\ \hat{C} \end{bmatrix} + \begin{bmatrix} \hat{C}(4\hat{C}+1)H\hat{\mu}^{k-2} & \hat{C}(4\hat{C}+1)H\hat{\mu}^{k-2} & 4\hat{C}H\hat{\mu}^{k-1} \\ \hat{C}(4\hat{C}+1)H\hat{\mu}^{k-2} & \hat{C}(4\hat{C}+1)H\hat{\mu}^{k-2} & 4\hat{C}H\hat{\mu}^{k-1} \\ 4\hat{C}\hat{\mu}^{k-1} & 4\hat{C}\hat{\mu}^{k-1} & \hat{\mu}^k + (\hat{\mu} - \hat{\alpha})^k \end{bmatrix} \begin{bmatrix} \|\delta {x_f}^{(0)}\| \\ \|\delta {x_s}^{(0)}\| \\ \|\delta {y_s}^{(0)}\| \end{bmatrix}
$$

with $\hat{\mu} = \hat{\alpha} + \frac{2CH}{\frac{\hat{\alpha}}{2C} + \sqrt{H}}$

[3] This requires non-singular Jacobians, see [2,8] for more details

Proof (of Lemma 2) Although the successive values of $(x_f{}^{(k)}, x_s{}^{(k)}, y_s{}^{(k)})$ remain in the neighborhood $\mathscr{U}_{\gamma_0}$ of the solution, **Lemma 1** shows that iteration error is mainly governed by the matrix:

$$\mathbf{J} = \begin{bmatrix} CH & CH & CH \\ CH & CH & CH \\ C & C & \hat{\alpha} + CH \end{bmatrix} \tag{33}$$

Recursive application of **Lemma 1** leads to:

$$\begin{bmatrix} \|\delta x_f{}^{(k)}\| \\ \|\delta x_s{}^{(k)}\| \\ \|\delta y_s{}^{(k)}\| \end{bmatrix} \leqslant \mathbf{J}^k \begin{bmatrix} \|\delta x_f{}^{(0)}\| \\ \|\delta x_s{}^{(0)}\| \\ \|\delta y_s{}^{(0)}\| \end{bmatrix} + \sum_{i=0}^{k-1} \mathbf{J}^i \begin{bmatrix} \|\delta \Delta x_f{}^{(0)}(T_N)\| \\ \|\delta \Delta x_s{}^{(0)}(T_N)\| \\ 0 \end{bmatrix} \tag{34}$$

Hence, the goal is to express in a relatively simple way the bounds for the elements of $\mathbf{J}^k$ and for the first column of $\sum \mathbf{J}^i$. The classical method used to obtain such bounds seeks to first transform the matrix into corresponding diagonal form $\mathbf{J}$ and then to bound the power of the eigenvalues. This leads to tedious but straightforward calculations; for more details the reader is invited to consider the Lemma 3.2. in [2].

Proof (of Theorem 1) The errors on the interest variables like $\varepsilon_{x_f,N}$ on x_f for the fluid part, $\varepsilon_{x_s,N}$ on x_s for the structure part, and $\varepsilon_{y_s,N}$ on y_s used for the coupling, are split in two terms: $e_{.,N+1}$ representing error propagation from one window N ($t \in [T_{N-1}, T_N]$) to the next $N+1$ ($t \in [T_N, T_{N+1}]$); $d_{.,N+1}$ corresponds to local error contribution on the window of interest $N+1$.

The proof is organized as follows: applying **Lemma 2** with suitable arguments, yields estimates for error propagation e (see proof (i)) and local error d (see proof (ii)). Then these estimates are combined to bounds set for the global errors ε (see proof(iii)). We can then show by induction that the global error bound is always verified (see proof (iv)). The constants μ and α are explicitly stated at the end of the proof of **Theorem 1** (v).

(i) Estimate of propagation error contribution is the first part of the proof, where **Lemma 2** with the following suitable arguments is applied:

$$\begin{bmatrix} \tilde{x_f}^{(0)} \\ \tilde{x_s}^{(0)} \\ \tilde{y_s}^{(0)} \end{bmatrix} \longleftarrow \begin{bmatrix} x_f{}_N^{(k_{\max})} \\ x_s{}_N^{(k_{\max})} \\ y_s{}_N^{(k_{\max})} \end{bmatrix} \quad \text{and} \quad \begin{bmatrix} x_f{}^{(0)} \\ x_s{}^{(0)} \\ y_s{}^{(0)} \end{bmatrix} \longleftarrow \begin{bmatrix} x_f{}_N^{\star} \\ x_s{}_N^{\star} \\ y_s{}_N^{\star} \end{bmatrix} \tag{35}$$

The symbol, '$\longleftarrow$' indicates the initial guesses (obtained with zero-th, first or second order predictors) from one window N to the next one $N+1$. For instance, in the simplest predictor is the constant function that leads to an error of size $\mathscr{O}(H)$:

$$(x_f{}_{N+1}^{(0)}, x_s{}_{N+1}^{(0)}, y_s{}_{N+1}^{(0)}) = (x_f{}_N^{(k_{\max})}, x_s{}_N^{(k_{\max})}, 0)$$

The values $(x_f{}_N^{(k_{\max})}, x_s{}_N^{(k_{\max})}, y_s{}_N^{(k_{\max})})$, in equation (35) above, obtained by numerical integration on the previous window N, can be considered as the best representation of the exact solution of the problem $(x_f{}_N^{\star}, x_s{}_N^{\star}, y_s{}_N^{\star})$ on this window. The choice of initial values (35) gives by definition the propagation error in the $N+1$-th windows for the (k)-th iteration: $\delta x_f{}^{(k)} = e_{x_f,N+1}$, $\delta x_s{}^{(k)} = e_{x_s,N+1}$ and $\delta y_s{}^{(k)} = e_{y_s,N+1}$.

It is assumed that the chosen initial guess operator $\longleftarrow$ satisfies Lipschitz condition:

$$\exists L^* \in \mathbb{R} \quad \text{such that} \quad \begin{cases} \|\Delta x_f{}^{(0)}\| \leqslant L^* \|\varepsilon_{x_f,N}\| \\ \|\Delta x_s{}^{(0)}\| \leqslant L^* \|\varepsilon_{x_s,N}\| \\ \|\Delta y_s{}^{(0)}\| \leqslant L^* \|\varepsilon_{y_s,N}\| \end{cases} \tag{36}$$

It will extrapolate x_f and x_s continuously from one window to another: $\|\delta x_f{}^{(0)}(T_N)\| \leqslant \|\varepsilon_{x_f,N}\|$ and $\|\delta x_s{}^{(0)}(T_N)\| \leqslant \|\varepsilon_{x_s,N}\|$. Therefore, the application of **Lemma 2** to the (k)-th iteration on window N with $\alpha < 1$ and a window size H small enough so that $\mu < 1$ leads to:

$$\begin{bmatrix} \|e_{x_f,N+1}\| \\ \|e_{x_s,N+1}\| \\ \|e_{y_s,N+1}\| \end{bmatrix} \leqslant \begin{bmatrix} 1+C_1^*H & 1+C_1^*H & C_1^*H \\ 1+C_1^*H & 1+C_1^*H & C_1^*H \\ C_1^* & C_1^* & \alpha^* \end{bmatrix} \begin{bmatrix} \|\varepsilon_{x_f,N}\| \\ \|\varepsilon_{x_s,N}\| \\ \|\varepsilon_{y_s,N}\| \end{bmatrix} \tag{37}$$

with $C_1^* \in \mathbb{R}_+$ and $\alpha^* := L^*(\hat{\mu}^k + (\hat{\mu} - \hat{\alpha})^k)$.

(ii) Estimate of local error contribution consists again in applying **Lemma 2** with suitable arguments:

$$\begin{bmatrix} \tilde{x_f}^{(0)} \\ \tilde{x_s}^{(0)} \\ \tilde{y_s}^{(0)} \end{bmatrix} \longleftarrow \begin{bmatrix} x_{f_N}^\star \\ x_{s_N}^\star \\ y_{s_N}^\star \end{bmatrix} \quad \text{and} \quad \begin{bmatrix} x_f{}^{(0)} \\ x_s{}^{(0)} \\ y_s{}^{(0)} \end{bmatrix} = \begin{bmatrix} x_{f_{N+1}}^\star \\ x_{s_{N+1}}^\star \\ y_{s_{N+1}}^\star \end{bmatrix} \tag{38}$$

Since the solution of the problem $(x_{f_n}^\star, x_{s_n}^\star, \lambda_n^\star)$ is a fixed-point of the iteration sequence, the local error contributions are measured by $(\delta x_f{}^{(k)}, \delta x_s{}^{(k)}, \delta y_s{}^{(k)}) = (d_{x_f,N+1}, d_{x_s,N+1}, d_{\lambda,N+1})$. Furthermore, the use of the solution of the problem as the initialization of the iterative sequence yields $(\delta x_f{}^{(0)}, \delta x_s{}^{(0)}, \delta y_s{}^{(0)}) = (\Delta x_f{}^{(0)}, \Delta x_s{}^{(0)}, \Delta y_s{}^{(0)})$, $\tilde{x_f}^{(0)}(T_N) - x_f{}^{(0)}(T_N) = 0$ and $\tilde{x_s}^{(0)}(T_N) - x_s{}^{(0)}(T_N) = 0$. Thus the application of **Lemma 2** then gives:

$$\begin{bmatrix} \|d_{x_f,N+1}\| \\ \|d_{x_s,N+1}\| \\ \|d_{y_s,N+1}\| \end{bmatrix} \leqslant \\ \left(\hat{\mu}^{k-2}\left(\|\Delta x_f{}^{(0)}\| + \|\Delta x_s{}^{(0)}\|\right) + \hat{\mu}^{k-1}\|\Delta\lambda^{(0)}\|\right) \begin{bmatrix} C_2^*H \\ C_2^*H \\ C_2^* \end{bmatrix} \tag{39}$$

with a positive constant C_2^*.

(iii) these estimates are combined with the bounds set for the global errors $\|\varepsilon_{N+1}\| \leqslant \|\mathbf{e}_{N+1}\| + \|\mathbf{d}_{N+1}\|$:

$$\begin{bmatrix} \|\varepsilon_{x_f,N+1}\| \\ \|\varepsilon_{x_s,N+1}\| \\ \|\varepsilon_{y_s,N+1}\| \end{bmatrix} \leqslant \begin{bmatrix} 1+C_1^*H & 1+C_1^*H & C_1^*H \\ 1+C_1^*H & 1+C_1H^* & C_1^*H \\ C_1^* & C_1^* & \alpha^* \end{bmatrix} \begin{bmatrix} \|\varepsilon_{x_f,N}\| \\ \|\varepsilon_{x_s,N}\| \\ \|\varepsilon_{y_s,N}\| \end{bmatrix} \\ + \left(\hat{\mu}^{k-2}\left(\|\Delta x_f{}^{(0)}\| + \|\Delta x_s{}^{(0)}\|\right) + \hat{\mu}^{k-1}\|\Delta y_s{}^{(0)}\|\right) \begin{bmatrix} C_2^*H \\ C_2^*H \\ C_2^* \end{bmatrix} \tag{40}$$

If the contraction condition $\alpha^* < 1$ is fulfilled, the behavior of such coupled error recursions is known (see [15], Lemma 2) and can be written as follows:

$$\max_N \left(\|\varepsilon_{x_f,N}\| + \|\varepsilon_{x_s,N}\| + \|\varepsilon_{y_s,N}\|\right) \\ \leqslant C \cdot \max_N \left(\hat{\mu}^{k-2}\left(\|\Delta x_f{}^{(0)}\| + \|\Delta x_s{}^{(0)}\|\right) + \hat{\mu}^{k-1}\|\Delta y_s{}^{(0)}\|\right) \tag{41}$$

with a positive constant C.

As the total error is the expressed by the sum $\|\varepsilon_{x_f,N}\| + \|\varepsilon_{x_s,N}\| + \|\varepsilon_{y_s,N}\|$, the last expression completes the proof of **Theorem 1**.

(iv) As the initial guess operator $\longleftarrow$ leads to initial errors $\|\Delta {x_f}^{(0)}\|$, $\|\Delta {x_s}^{(0)}\|$ and $\|\Delta {y_s}^{(0)}\|$ of size $\mathscr{O}(H)$, the right-hand side of the last equation remains bounded for all $H < H_0$, if H_0 is sufficiently small:

$$\begin{aligned} &\max_N \left(\|\varepsilon_{x_f,N}\| + \|\varepsilon_{x_s,N}\| + \|\varepsilon_{y_s,N}\| \right) \\ &\leqslant C \cdot \max_N \left(\hat{\mu}^{k-2} \left(\|\Delta {x_f}^{(0)}\| + \|\Delta {x_s}^{(0)}\| \right) + \hat{\mu}^{k-1} \|\Delta \lambda^{(0)}\| \right) \\ &\leqslant \gamma_0 \end{aligned} \tag{42}$$

This further shows that errors is bounded by γ_0, and that approximate numerical solution remains in the neighborhood $\mathscr{U}_{\gamma_0}$ of the solution.

(v) The constants $\hat{\alpha}$ and $\hat{\mu}$ which appear in proofs of **Lemma 1** and **Lemma 2** are given as follows:

$$\hat{\alpha} = \alpha + \mathscr{O}(1) \max_n (\|\varepsilon_{x_f,N}\| + \|\varepsilon_{x_s,N}\| + \|\varepsilon_{\lambda,N}\|) + \mathscr{O}(H) = \alpha + \mathscr{O}(H)$$

and

$$\hat{\mu} = \hat{\alpha} + \mathscr{O}(H)$$

These results give the following order of magnitude for α^*:

$$\alpha^* = L^*(\hat{\mu}^k + (\hat{\mu} - \hat{\alpha})^k) = L^*((\alpha + \mathscr{O}(H)^k + \mathscr{O}(H^k)) \tag{43}$$

The expression above confirms the criterion of stable error propagation for $\alpha^* < 1$. For the iterative DFMT-BGS with an appropriate guess operator, the stability is guaranteed when $\alpha < 1$ and when the window size is small enough.

5 Validation and numerical examples

5.1 Lid-driven cavity flow with flexible bottom

Having recognized the value of this problem for establishing the standard benchmark in fluid-structure interaction, we will provide a sufficiently detailed presentation of the results obtained in order to promote the comparison.

The lid-driven cavity flow considers 2D fluid flow problem in a square domain. The imposed boundary conditions at three out of four sides are the zero value of velocity. Only at the top of the cavity we impose the velocity with a given nonzero value. The geometry and boundary conditions are depicted in further details in Figure 3.

For the case of fluid-structure interaction problem [59,26] the flexible membrane is placed at the bottom boundary (see Figure 3(b)). The flow is governed with Navier-Stokes equations and we consider a Saint-Venant Kirchoff material able to undergo finite deformation for the structure part. The material properties are chosen as follows: the fluid density is $\rho_f = 1kg \cdot m^{-3}$, the kinematic velocity $\nu_f = 0.01m \cdot s^{-2}$, the structure density is $\rho_s = 500kg \cdot m^{-3}$, the Young modulus $E = 250Pa$ and the Poisson ratio $\nu = 0$.

The flow has a dominant convective term, which is usually the most difficult to solve accurately. Furthermore, when the imposed velocity is sufficiently small, the flow is laminar and incompressible. In fact, this lid-driven cavity flow (with a rigid bottom) problem is traditionally used as a validating example for CFD codes. Therefore extensive literature is

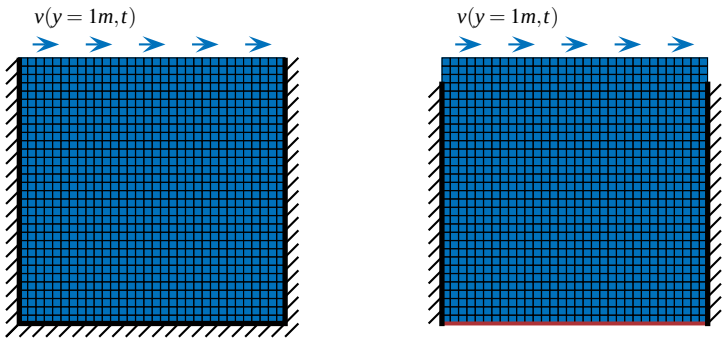

(a) Lid-driven fluid flow in cavity (b) Modified lid-driven cavity for FSI

Fig. 3 The lid-driven cavity example

dedicated to its study, ever since the early works in computational fluid dynamics [27] to more recent reviews [9] using different fluid solvers [29,22]. It is also proposed as a test case for the fluid solver of `OpenFOAM` [48] we employ in this work. In the present test, the cavity is discretized by finite volume mesh of 32×32 cells.

For the lid-driven cavity flow in Figure 3(a), all boundary nodes are constrained at the Dirichlet boundary with imposed velocity, and pressure field remains undetermined up to a constant. If this does not lead to any problem when only fluid flow is considered with no interaction with the structure, a special care has to be taken for the fluid-structure interaction case where the imposed velocity condition should satisfy incompressibility condition and where the exact value of pressure is needed to define structure boundary conditions. This difficulty was studied in [39].

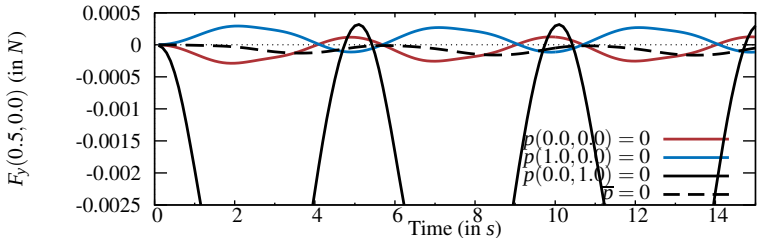

Fig. 4 Force acting at the center of the flexible bottom for some fixing pressure strategies

One way to overcome this difficulty for fluid-structure interaction lid-driven cavity problem, as proposed in [59,39] is to unconstrain two nodes on each size of the cavity (see Figure 3(b)). One subtle point concerns the chosen discretization techniques: for stabilized FE approximation used in [59,39] constraints are removed at the nodes, whereas for the FV method used herein the corresponding constraints at the boundary pertain to face of cells. Another modification of lid-driven cavity problem, besides taking into account the fluid-

structure interaction, concerns the time-dependent velocity boundary condition defined as:

$$v \cdot e_x = 1 - \cos\left(2\pi \frac{t}{T_{\text{char}}}\right) \tag{44}$$

where $T_{\text{char}} = 5s$. For such harmonic function, the solution of the fluid flow within the fluid-structure interaction problem exhibits an oscillating behavior that is reached after a short transition period. The maximum value of the Reynolds number in the cavity reaches $\mathscr{R}e = 200$, and thus the flow can be considered as laminar.

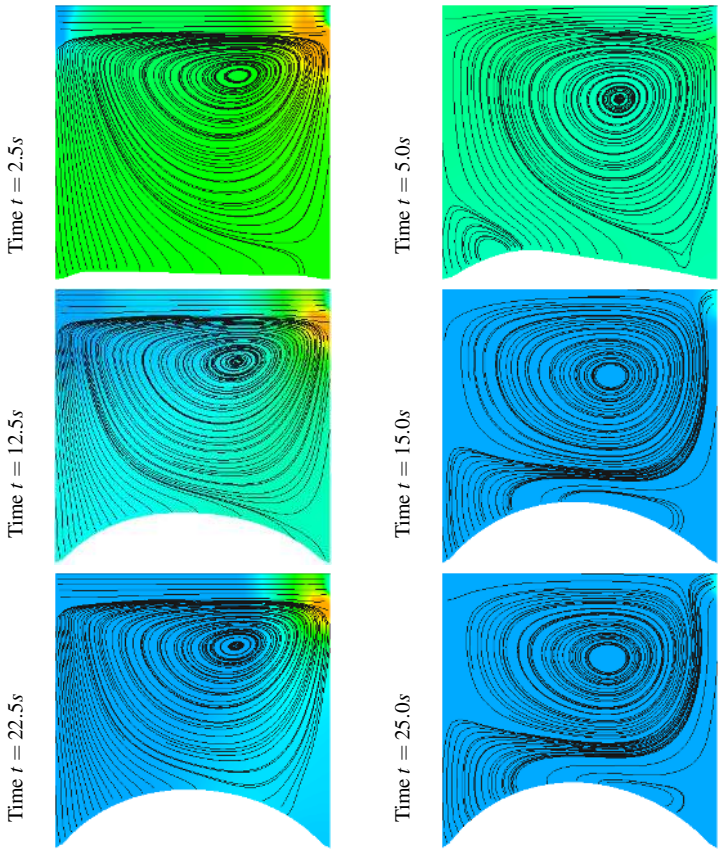

Fig. 5 Lid driven cavity with a flexible bottom: snapshots with pressure field and streamlines for different time steps

This example represents a very good benchmark test for the case when the flow is mainly driven by incompressibility. Moreover, it allows to obtain pretty good results with a rather coarse mesh; namely with the Reynolds number not bigger than $\mathscr{R}e = 200$, a mesh with 32x32 cells and a second order FV solver is sufficient to get an accurate solution [27,29]. Due to such a small mesh size, computations are fairly inexpensive, especially for a fluid-structure interaction problem (for each time step of $\Delta t = 0.1s$, the flow computation takes

$1.08 \times 10^{-1} s$ and the structure motion takes $2.95 \times 10^{-3} s$ when run on a single processor). The problem quickly reaches a harmonic steady-state solution, which provides a perfect platform to test the energy creation or dissipation for partitioned solution to fluid-structure interaction problem.

For the fluid flow only, we can stick with the problem where boundary conditions are imposed on the velocity field, with no condition on the pressure field p. These boundary conditions are also called zero gradient (or Neumann zero). In this case any constant can be added to the computed pressure field, with no change for the fluid part since the gradient of the pressure field in (9) will filter out any constant pressure. However, this can lead to a non-unique pressure, and most of the iterative solver will fail for such a problem if no remedy is proposed. This is even a bigger problem for fluid-structure interaction, where the exact pressure is needed to obtain the corresponding structural motion.

If the fluid flow case only is considered there are two possible modifications (see [22]) of this problem in order to specify a unique pressure field for Neumann zero boundary. Namely, we can impose either the fixed value (*e.g.* zero) of the pressure in a arbitrary cell, or we can consider the pressure field with the mean value equal to an imposed constant.

However, for the present version of the lid-driven cavity that accounts for fluid-structure interaction problem, the issue of pressure computation becomes more demanding since not only the gradient of the pressure field, but also its actual values must be known at the fluid-structure interface. Unfortunately, a number of previous works (see [60,39,26]) did not clearly specify the imposed condition on the pressure field. For example in [4], where the pressure field is imposed at the flow inlet and outlet, the obtained result is totally different from the one given by the previous works predicting a high pressure at the bottom of the cavity leading to an average negative displacement of the structure in the e_y direction, and requiring the use of a stiffer material in order to remain in the acceptable displacement range.

In order to illustrate the importance of the chosen pressure condition in fluid-structure interaction analysis we take the case of an almost rigid structure at the bottom and compute the total force (from pressure and viscosity) applied to its center (nodal force at $(0.5, 0.0)$). These results are presented in Figure 4, showing very different time evolutions of pressure force exerted on the structure for different choices of pressure boundary conditions. For further computations, the pressure was set to zero at the flow outlet. Other boundaries are considered to be Neumann zero for the pressure. The fluid domain is discretized with fourth order FV in space, and the time integration is carried out by implicit Euler scheme. The momentum equation is solved by PBiCG, with a DILU preconditioning whereas the pressure correction problem is worked out by iterative PCG, with DIC preconditioning. Two iterations of the PISO correction algorithm are performed at each time step, and the precision required for the iterative algorithms for pressure and velocity is 10^{-8}. As the mesh is initially orthogonal, there is no reason to require initially non-orthogonal correctors. At a later stage the deformation of the bottom will eventually produce non-orthogonal meshes and we specify that two non-orthogonal corrections should be performed at each time step.

The fluid domain is subject to structure motion as the bottom of the domain. We assume that no cavitation takes place and that fluid follows the deformation of the structure. The fluid mesh deformation is handled by a smoothing process, based upon the solution to Laplacian equation with the coefficient that depends on the distance to the bottom. On vertical walls, the points are allowed only to move vertically, whereas elsewhere the boundary nodes are fixed.

For the structure FE model a spatial discretization with $16\times$Q8 (quadratic) elements is chosen. The time integration is carried out by implicit generalized HHT α-scheme in

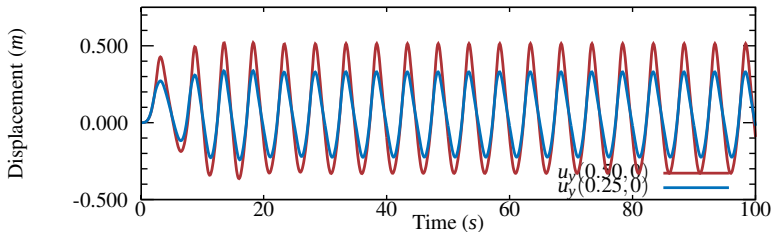

Fig. 6 Displacements at the fluid-structure interaction interface at the middle and the quarter lengths: $u(0.5,0)$ and $u(0.25,0)$.

order to maximize numerical damping [24]. The non-linear algebraic equations is solved at each time step by the Newton iterative algorithm with a prescribed tolerance of 10^{-8}. A non-symmetrical direct solver is used at each iteration.

The typical results for the pressure field, streamlines and structure deformation are plotted in Figure 5. In Fig 6 the time history of the displacement is displayed when no interaction is considered. Namely, the forces are computed by the CFD-based component, and applied to the structure, but the structure motion is not imposed on the fluid domain, and thus there is no need to compute any mesh motion. The same kind of results are presented in Figure 7 for implicit coupling computations with a window size of $\Delta t = 0.1s$. The results largely differ from the one obtained with a weak interaction model. The displacement remains exactly the same for all predictors and relaxation techniques, once convergence to a residual norm less than 10^{-7} is obtained. The results are close to those obtained in [59, 26, 39] (see Figure 7(b)).

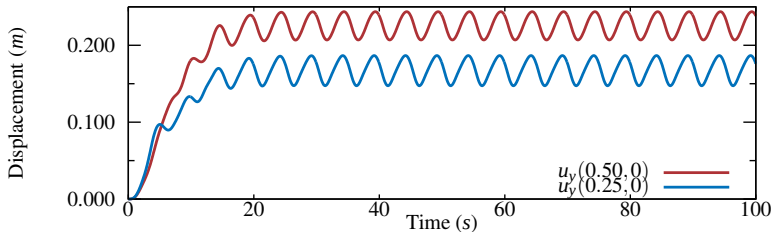

(a) Displacements at the fluid-structure interaction interface at the middle and the quarter lengths: $u(0.5,0)$ and $u(0.25,0)$.

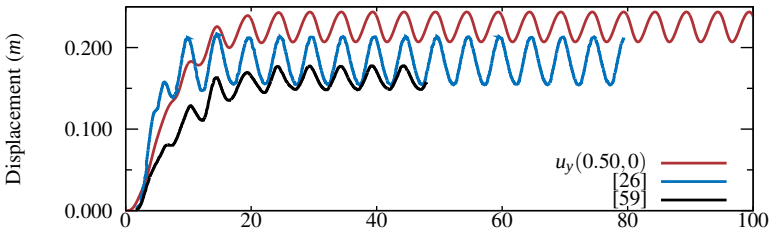

(b) Displacement of the flexible bottom center compared with results from [59] (DFMT-BGS coupling FEM for structure and stabilized FEM for fluid) and [26] (DFMT-BN coupling FEM for structure and stabilized FEM for fluid)

Fig. 7 Implicit computation of the lid-driven cavity with flexible bottom solved with BGS and relaxation.

Note that the inertia of the flexible bottom leads to a positive mean value of structure displacement. Moreover, this further induces a large decrease in pressure and accordingly in the expected force amplitude.

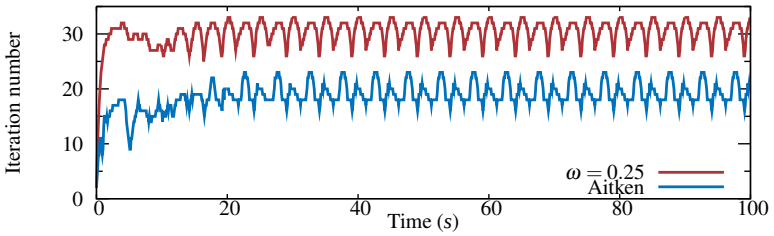

Fig. 8 Number of iterations per time step for the BGS solver with fixed and Aitken's relaxation (order 0 predictor)

A tolerance $\texttt{TOL} = 10^{-7}$ is set for testing the convergence of the DFMT-BGS algorithm. With a fixed under-relaxation of $\omega = 0.25$, a constant decrease of the residual with a low order is observed (see Figure 10). Aitken's relaxation allows to reduce the mean number of iterations required from 30 to 17 (see Figure 8). Aitken's relaxation allows also to improve the order of convergence. The convergence exhibits a less smooth behavior, with a faster decrease of the residual with the increase of relaxation parameters (for instance the 4^{th} iteration in Figure 12(a) and 10(a)). The relaxation parameter value is given in Figure 12 for two chosen times $39s$ and $41s$ used in Figure 10 to represent the convergence of the residual; The characteristic oscillations depicted in [40] are also observed.

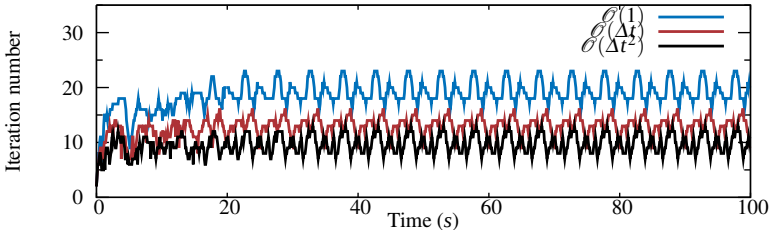

Fig. 9 Number of iterations per time step for the BGS solver with predictor of order 0, 1 and 2 (Aitken's relaxation)

The use of predictors does not change the order of convergence, but reduces the initial residual (see Figure 11). For example the characteristic number of iterations to reach required precision decreases from 17 iterations for a zero order to 7 for a second order predictor (Figure 9).

At the end of this section, we also present the results obtained for explicit DFMT coupling algorithms applied to the lid-driven cavity with flexible structure at the bottom. The added mass effects characteristic of explicit algorithms for the case of an incompressible flow is observed in Figure 13, causing each computation to diverge sooner or later.

Our result divergence was not in agreement with the results convergence presented in [24] for the least accurate predictors. The main reason, we believe, is due to the way the enforcement of the true incompressibility condition for the fluid problem is really enforced.

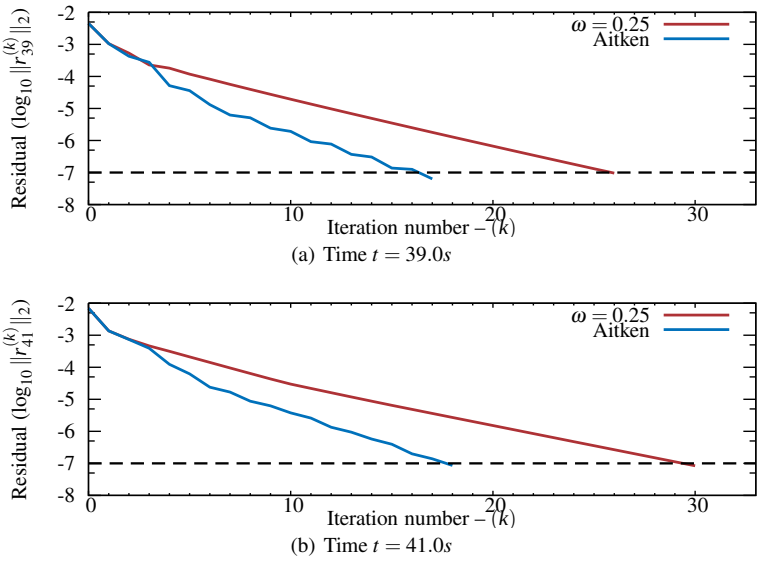

Fig. 10 Residual convergence for fixed and Aitken's relaxation with order 0 predictor

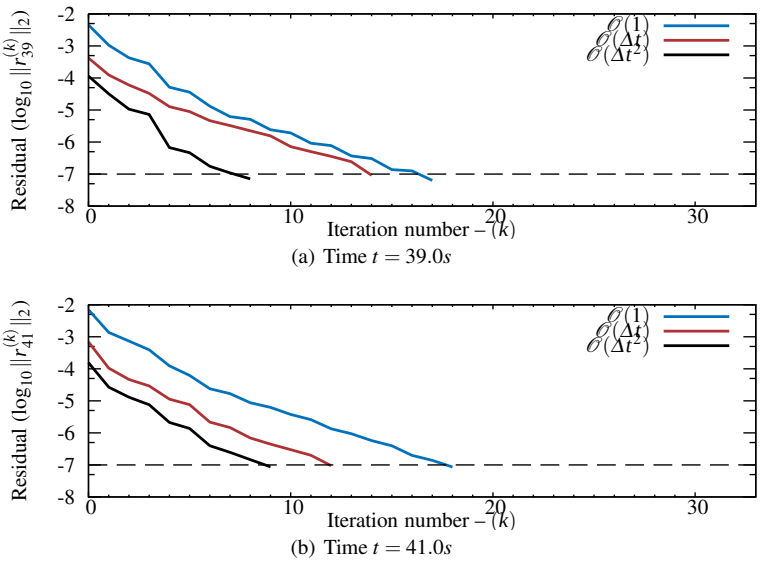

Fig. 11 Residual convergence with Aitken's relaxation and predictor of order 0, 1 and 2

Namely, with FV and PISO algorithm used herein, we can strongly enforce incompressibility condition, which is less the case when using stabilized FE discretization as in [24].

The choices recognized to be important for triggering earlier instability of explicit coupling are: increasing the order of predictor (see Figure 13(a)), decreasing the window size for synchronization, (see Figure 13(b)), increasing the order of fluid integrator, (see Figure 13(c)), use of non-collocated algorithm like the DFMT-ISS (see Figure 13(d)). Mass

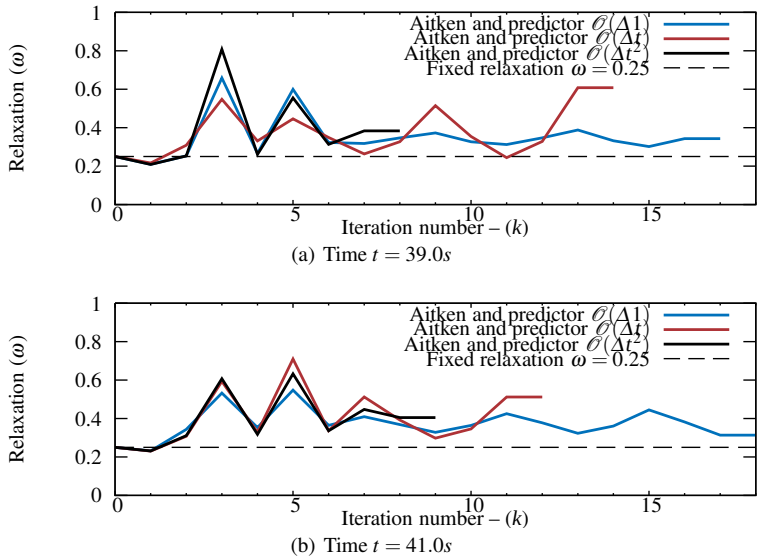

(a) Time $t = 39.0s$

(b) Time $t = 41.0s$

Fig. 12 The lid-driven: evolution of relaxation parameter for two characteristic time steps

ratio between fluid and solid with larger ρ_f/ρ_s, the instability occurs earlier; larger fluid velocities and more flexible structure trigger instability more quickly. This is in fully agreement with the theoretical and numerical observations made in [10,24,23]. The general conclusion is that accurate time integration of the sub-problem and coupling algorithms are more sensitive to the artificial "Added-Mass Effect" and diverge more easily.

5.2 Flexible appendix in a flow

This example first proposed in [60], and subsequently also studied in [14,30,43] has also been used as a benchmark for fluid-structure interaction. It is close to the benchmark proposed in [58] itself constructed from the traditional CFD benchmark proposed in [53].

We consider a fixed square bluff body, with a flexible appendix attached to it, immersed within an incompressible flow (see Figure 14) filling the whole domain. At a sufficiently long distance from this body, the flow is uniform with an imposed velocity $\bar{v}$; the corresponding value of the Reynolds number with respect to the characteristic size of the obstacle is $\mathscr{R}e = 330$. For this Reynolds number, the flow exhibits a transient behavior with vortices separating from the corner of the square. These vortices induce alternative drop and increase in the pressure field behind the rigid bluff body at a frequency that depends on the Reynolds number and the shape of the bluff body [51]. The vortex shedding induces oscillations of the flexible appendix.

The thickness of the appendix as well as the material properties are chosen so that its first eigen-frequency is close to the frequency of the vortex shedding. The material parameters are respectively $\rho_f = 1.18 \times 10^{-3} kg.m^{-3}$ for the density and $\nu_f = 1.54 \times 10^{-1} m^2.s^{-1}$ for the for the fluid (air at 20°C). The imposed velocity at the left hand side is $\bar{v} = (51.3m.s^{-1}, 0)$.

For the solid part, consider a density $\rho_s = 0.1kg.m^{-3}$, Young modulus is of $E_s = 2.5 \times 10^6 N.m^{-2}$ and the Poisson ratio coefficient of $\nu_s = 0.35$. The first eigen-frequency of the

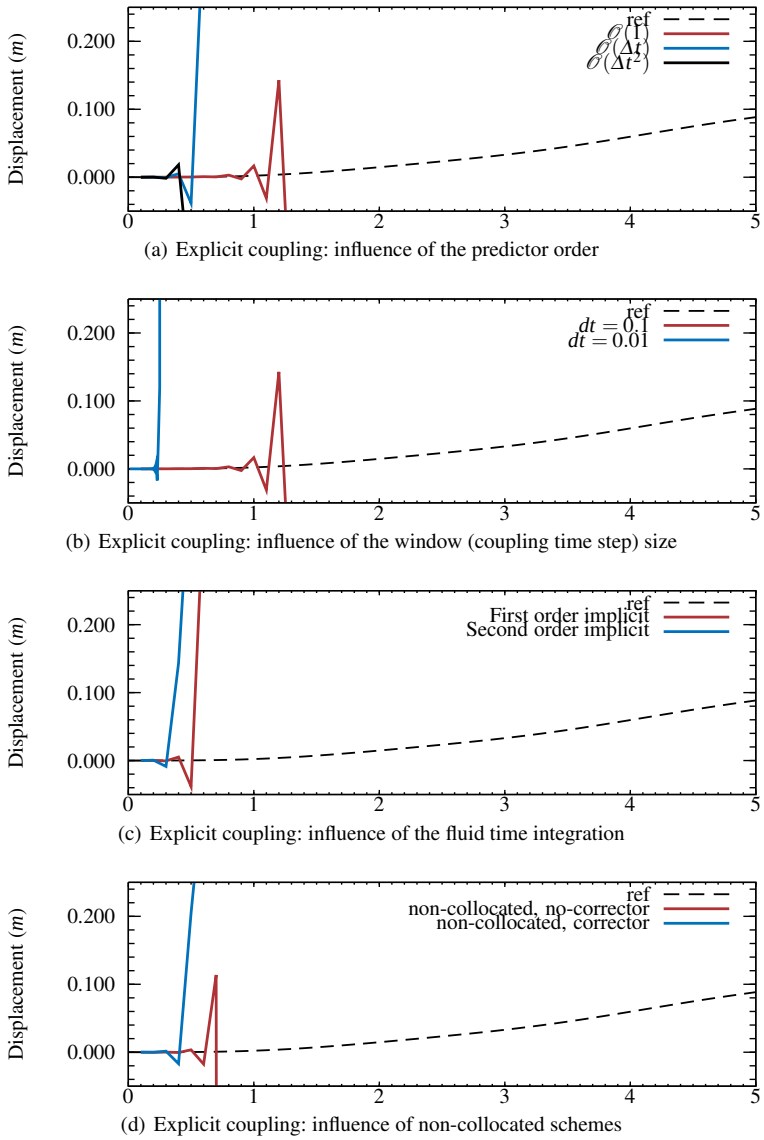

(a) Explicit coupling: influence of the predictor order

(b) Explicit coupling: influence of the window (coupling time step) size

(c) Explicit coupling: influence of the fluid time integration

(d) Explicit coupling: influence of non-collocated schemes

Fig. 13 Divergence of the explicit coupling for different coupling algorithm and time integration schemes

problem $f = 3.03s^{-1}$ obtained considering a linear material is closed to the natural frequency of vortex shedding behind a square bluff body at Reynolds $\mathscr{R}e = 330$.

The chosen fluid discretization contains 5080 FV cells (i.e. around 20×10^3 d-o-f), which is quite sufficient to get an accurate representation of the flow, and also of the fluid loading on the structure. The model accuracy is comparable to the one used in [14], built with 4300 finite elements. The PISO algorithm and the Euler implicit scheme with a time step $\Delta t = 0.004s$ are used. The PCG solver is used for pressure correction step and mesh motion equations and PBiCG for the momentum predictor.

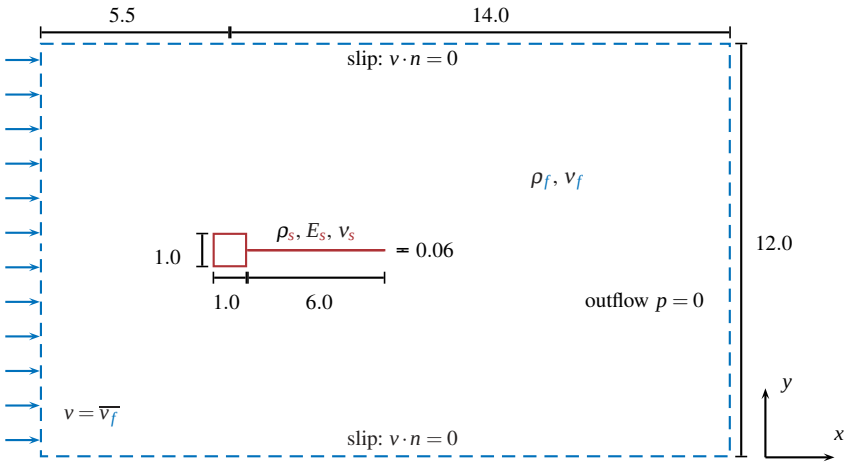

Fig. 14 The benchmark used for FSI problems

The flexible appendix is discretized with 20 nine-node elements, with quadratic polynomes description of large structural displacement. Neo-Hookean and Saint-Venant–Kirschoff materials are used. The time discretization is carried out by a generalized HHT-α scheme with the following parameters: $\rho_\infty = \frac{1}{2}; \beta = \frac{4}{9}; \gamma = \frac{5}{3}$; and $\alpha = \frac{2}{3}$ At each iteration, the linear system is solved by the direct solver for asymmetric matrices.

The interface matching computation is carried out by the proposed DFMT-BGS solver, that can easily converge since the channel is open and the flow is not mainly driven by incompressibility. The Aitken relaxation technique is used with an initial value of 0.5, that rapidly increases to 1. No more than 4 iterations are required to reach the required tolerance on the interface displacement residual that is set to 1×10^{-7}. The results for pressure and velocity field at several instants are given in Figure 15. The deformed shapes of the appendix also given in Figure 15, reveal the oscillations dominated by the first mode.

The displacement at the free-end of the appendix is plotted in Figure 16 for both Saint-Venant–Kirschoff and Neo-Hookean solid materials. The two results are very close, since the appendix deformations remain small, despite its large displacement and rotations. The long term response (see Figure 17) indicates an almost harmonic response dominated by the first eigen-frequency of the structure. In Figure 17 we also give a comparison with the results from the literature in term of the maximum amplitude of motion. Despite a well-known sensitivity of the computed result with respect to the initial condition [30], we get the answers obtained very close to the previous results from the literature based upon a FE discretization for both fluid and solid parts and obtained either by a monolithic [14] or a partitioned approach [59,44].

Contrary to the lid-driven cavity with a flexible bottom, the small number of iterations required to solve the fluid-structure interaction problem of the oscillating appendix suggests that an explicit coupling can also be used for solving this problem. The results from explicit DFMT algorithm presented in Figure 18 for the free-end displacement compare to a reference solution obtained with an implicit computation.

Using better predictors is supposed to reduce the errors made in term of residual and energy. In Figure 19(b), the energy error time history is represented for the zero, first and

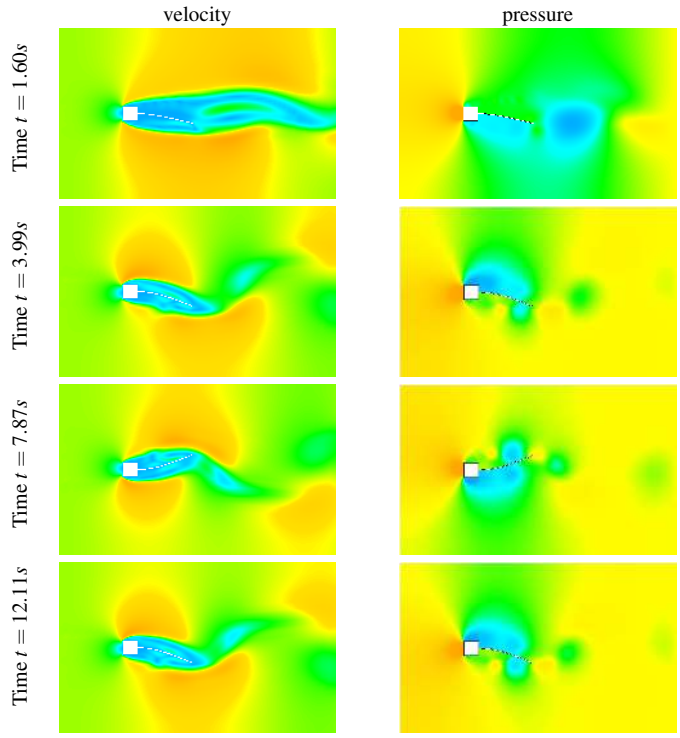

Fig. 15 Oscillating appendix in flow: velocity and pressure field snapshots

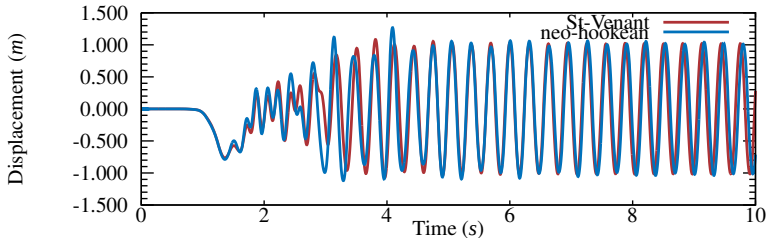

Fig. 16 Implicit coupling: displacement of the appendix extremity for two non-linear materials (Saint-Venant and Neo-Hookean)

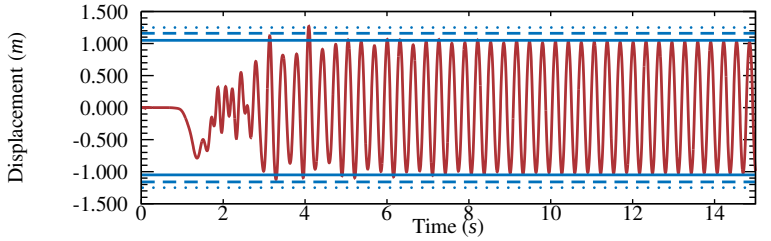

Fig. 17 Implicit coupling: long term response with implicit coupling. Maximum amplitude comparison with [14] (dotted line), [44] (solid line), [59] (dashed line).

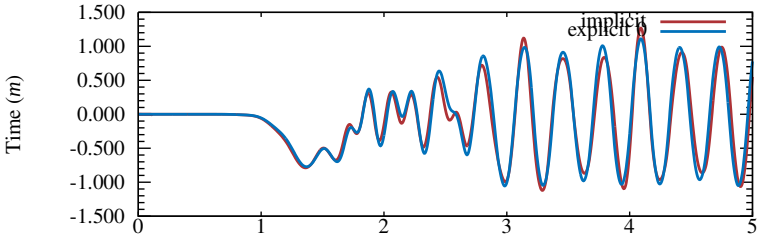

Fig. 18 Comparison between explicit and implicit coupling algorithm based computations for the displacement of the appendix.

second order predictor. All the results confirm the trends we expected, with a decrease of errors when the predictor order increases.

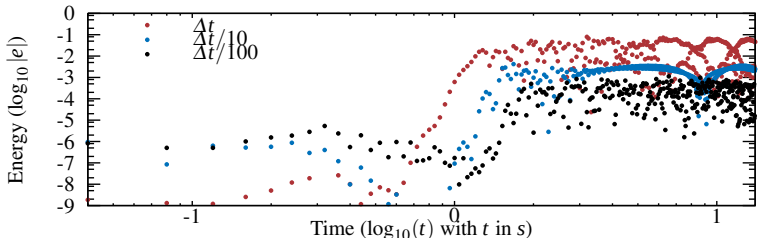

(a) Energy error for different time step size

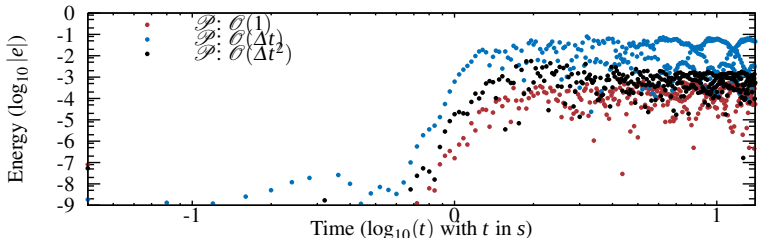

(b) Energy error for different predictors

Fig. 19 Energy error at the interface for different explicit coupling schemes.

The final study is then considered with respect to the size of time steps. In Fig 20, the maximum residual error on the time interval $t \in [0, 15s]$ is presented as a function of the time step size. The error is observed to decrease with a decreasing time step size. However, when the time steps become too small, the added mass effect triggers the divergence of the computation. Thus, only the less sensitive schemes with a zero order predictor are able to solve the coupled problem with the smallest time step.

Remark: The extension to three-dimensional cases does not require the introduction of theory, but requires tools to solve efficiently the problem with a large number of d-o-f, with the use of paralleling for instance. A generalization of the two dimensional case presented

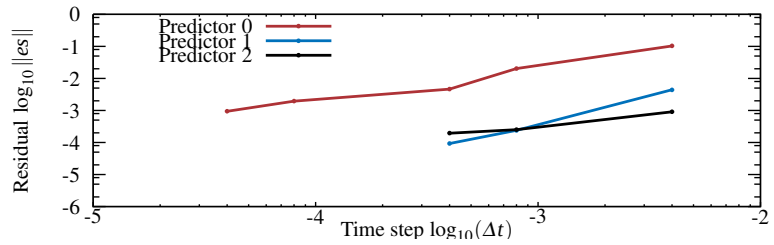

Fig. 20 Maximum residual error for explicit coupling schemes with different time step sizes and predictors.

herein (see Fig. 21) and other three-dimensional numerical examples are discussed in the Part II of this work.

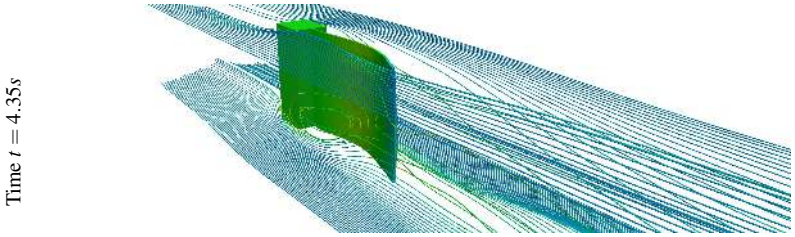

Fig. 21 Flag in the wind: motion of the structure and stream-tube snapshots.

6 Conclusion

In this work we examine partitioned solution approach for nonlinear fluid-structure interaction problems. The partitioned approach is preferred for its modularity and the possibility of re-using existing software developed for each subproblem (see Part II). The partitioned approach used here is based on the Direct Force-Motion Transfer. Both explicit and implicit coupling algorithms for multi-physics problems are detailed. An explicit strategy leads to the so-called "added mass effect", and for that justifies the use of more costly implicit solvers for the case of incompressible fluid flows.

In this work, the problem of enforcing the fluid-structure interface matching is handled by the fixed-point strategy (DFMT-BGS) with an adaptive relaxation parameter. This strategy shows a sufficiently robust performance, especially for the example where the flow is not highly constrained by incompressibility. In fact, we showed by direct proof the stability of the implicit DFMT-BGS algorithm which is valid for the fully nonlinear fluid-structure interaction problem.

References

1. M. Arnold. Constraint partitioning in dynamic iteration methods. *Zeitschrift fur Angewandte Mathematik und Mechanik*, 81:735–738, 2001.

2. M. Arnold and M. Gunther. Preconditioned dynamic iteration for coupled differential-algebraic systems. *BIT Numer. Math.*, 41:1–25, 2001.
3. Manuel Barcelos, Henri Bavestrello, and Kurte Maute. A Schur–Newton–Krylov solver for steady-state aeroelastic analysis and design sensitivity analysis. *Computer Methods in Applied Mechanics and Engineering*, 195:2050–2069, 2006.
4. Klaus-Jürgen Bathe and Hou Zhang. A mesh adaptivity procedure for CFD and fluid-structure interactions. *Computers and Structures*, 87(11-12):604–617, 2009.
5. T. Belytschko, H. J. Yen, and R. Mullen. Mixed methods for time integration. *Computer Methods in Applied Mechanics and Engineering*, 17(18):259–275, 1979.
6. Ted Belytschko. An overview of semidiscretization and time integration procedures. In Ted Belytschko and T. J. R. Hughes, editors, *Computational methods for transient analysis*, pages 1–65, Amsterdam, North-Holland, 1983. Journal of Applied Mechanics.
7. Ted Belytschko, Wing Kam Liu, and Brian Moran. *Nonlinear finite elements for continua and structures*. Wiley, New-York, 2000.
8. K. E. Brenan, S. L. V. Campbell, and L. R. Petzold. *Numerical solution of initial-value problems in Differential-Algebraic Equations*. Society for Industrial and Applied Mathematics, 1996.
9. Charles-Henri Bruneau and Mazen Saad. The 2D lid-driven cavity problem revisited. *Computers and Fluids*, 35:326–348, 2006.
10. P. Causin, J.-F. Gerbeau, and Fabio Nobile. Added-mass effect in the design of partitioned algorithms for fluid-structure problems. *Computer Methods in Applied Mechanics and Engineering*, 194(42-44):4506–4527, 2005.
11. Joris Degroote, Klaus-Jürgen Bathe, and Jan Vierendeels. Performance of a new partitioned procedure versus a monolithic procedure in fluid-structure interaction. *Computers and Structures*, 87(11-12):793–801, 2009.
12. I. Demirdžić and Milovan Perić. Space conservation law in finite volume calculations of fluid flow. *International Journal for Numerical Methods in Fluid*, 8(9), 1988.
13. Simone Deparis, Marco Discacciati, Gilles Fourestey, and Alfio Quarteroni. Fluid-structure algorithms based on Steklov-Poincaré operators. *Computer Methods in Applied Mechanics and Engineering*, 195(41-43):5797–5812, 2006.
14. W. G. Dettmer and Djordje Perić. A fully implicit computational strategy for strongly coupled fluid-solid interaction. *Archives of Computational Methods in Engineering*, 14:205–247, 2007.
15. P. Deuflhard, E. Hairer, and J. Zugck. One-step and extrapolation methods for differential-algebraic systems. *Numerische Mathematik*, 51:501–516, 1987.
16. Charbel Farhat and M. Lesoinne. Two efficient staggered algorithms for the serial and parallel solution of three-dimensional nonlinear transient aeroelastic problems. *Computer Methods in Applied Mechanics and Engineering*, 182:499–515, 2000.
17. Charbel Farhat, M. Lesoinne, and N. Maman. Mixed explicit/implicit time integration of coupled aeroelastic problems: three-field formulation, geometric conservation and distributed solution. *International Journal for Numerical Methods in Engineering*, 21(10), 1995.
18. C.A. Felippa and K.C. Park. Synthesis tools for structural dynamics and partitioned analysis of coupled systems. *NATO Advanced Research Workshop (eds. A. Ibrahimbegović and B. Brank)*, pages 50–111, 2004.
19. Carlos A. Felippa, K. C. Park, and J. A. de Runtz. Stabilization of staggered solution procedures for fluid-structure interaction analysis. In *Computational methods for fluid-structure interaction problems*, pages 95–124, 1977.
20. M. Á. Fernández, J.-F. Gerbeau, A. Gloria, and M. Vidrascu. Domain decomposition based Newton methods for fluid-structure interaction problems. In *ESAIM: Proceedings*, volume 22, pages 67–82. edpsciences.org, 2008.
21. M. Á. Fernández and M. Moubachir. A Newton method using exact Jacobians for solving fluid–structure coupling. *Computers and Structures*, 83(2-3):127–142, 2005.
22. Joel H. Ferziger and Milovan Perić. *Computational Methods for Fluid Dynamics*. Springler-Verlag, Berlin, Germany, 3rd edition, 2002.
23. Christiane Förster, Wolfgang A. Wall, and Ekkehard Ramm. On the geometric conservation law in transient ow calculations on deforming domains. *International Journal for Numerical Methods in Fluid*, 50:1369–1379, 2006.
24. Christiane Förster, Wolfgang A. Wall, and Ekkehard Ramm. Artificial added mass instabilities in sequential staggered coupling of nonlinear structures and incompressible viscous flows. *Computer Methods in Applied Mechanics and Engineering*, 196:1278–1291, 2007.
25. L. P. Franca, T. J. R. Hughes, and R. Stenberg. Stabilized finite element methods. *Incompressible Computational Fluid Dynamics*, pages 87–107, 1993.

26. J.F. Gerbeau and M. Vidrascu. A quasi-Newton algorithm based on a reduced model for fluid-structure interaction problems in blood flows. *Mathematical Modelling and Numerical Analysis*, 37(4):631–647, 2003.
27. U. Ghia, K. N. Ghia, and C. T. Shin. High-Re solutions for incompressible flow using the Navier-Stokes equations and a multigrid method. *Journal of Computational Physics*, 48:387–411, 1982.
28. M. Heil. An efficient solver for the fully coupled solution of large-displacement fluid–structure interaction problems. *Computer Methods in Applied Mechanics and Engineering*, 193(1-2):1–23, 2004.
29. M Hortmann, M Perić, and G Scheuerer. Finite volume multigrid prediction of laminar natural convection: Bench-mark solutions. *International Journal for Numerical Methods in Fluid*, 11:189–207, 1990.
30. Björn Hübner, Elmar Walhorn, and Dienter Dinkler. A monolithic approach to fluid-structure interaction using space-time finite elements. *Computer Methods in Applied Mechanics and Engineering*, 193:2087–2014, 2004.
31. T. J. R. Hughes, Wing Kam Liu, and T. K. Zimmermann. Lagrangian-Eulerian finite element formulation from incompressible viscous flows. In *Interdisciplinary Finite Element Analysis: Proceedings of the US-Japan Seminar Held at Cornell University*, page 179. College of Engineering and School of Civil & Environmental Engineering of Cornell University, 1981.
32. T. J. R. Hughes, K. S. Pister, and R. L. Taylor. Implicit-explicit finite elements in nonlinear transient analysis. *Computer Methods in Applied Mechanics and Engineering*, 17:159–182, 1979.
33. Adnan Ibrahimbegovic. *Nonlinear solid mechanics: Theoretical formulations and finite element solution methods*. Springer, 2009.
34. Adnan Ibrahimbegovic and Bostjan Brank. *Engineering Structures Under Extreme Conditions: Multi-physics and Multi-scale Computer Models in Non-linear Analysis and Optimal Design*. IOS Press, 2005.
35. Adnan Ibrahimbegovic and Said Mamouri. Energy conserving & decaying implicit time-stepping scheme for nonlinear dynamics of three-dimensional beams undergoing finite rotations. *Computer Methods in Applied Mechanics and Engineering*, 191:4241–4258, 2002.
36. M. M. Joosten, W. G. Dettmer, and Djordje Perić. Analysis of the block gauss-seidel solution procedure for a strongly coupled model problem with reference to fluid-structure interaction. *International Journal for Numerical Methods in Engineering*, 78(7), 2009.
37. Christophe Kassiotis, Jean-Baptiste Colliat, Adnan Ibrahimbegovic, and Hermann G. Matthies. Multiscale in time and stability analysis of operator split solution procedure applied to thermomechanical problems. *Engineering Computations*, 1-2:205–223, 2009.
38. Christophe Kassiotis, Adnan Ibrahimbegovic, Hermann G. Matthies, and Bostjan Brank. Stable splitting scheme for general form of associated plasticity including different scales of space and time. *Computer Methods in Applied Mechanics and Engineering*, In Press, Corrected Proof, 2009.
39. Ulrich Küttler, Christiane Förster, and Wolfgang A. Wall. A solution for the incompressibility dilemma in partitioned fluid-structure interaction with pure Dirichlet fluid domains. *Computational Mechanics*, 38:417–429, 2006.
40. Ulrich Küttler and Wolfgang A. Wall. Fixed-point fluid-structure interaction solvers with dynamic relaxation. *Computational Mechanics*, 43(1):61–72, 2008.
41. P. Le Tallec and J. Mouro. Fluid structure interaction with large structural displacements. *Computer Methods in Applied Mechanics and Engineering*, 190(24-25):3039–3067, 2001.
42. A. Legay, J. Chessa, and T. Belytschko. An eulerian-lagrangian method for fluid-structure interaction based on level sets. *Computer Methods in Applied Mechanics and Engineering*, 195(17-18):2070–2087, 2006.
43. Hermann G. Matthies, Rainer Niekamp, and Jan Steindorf. Algorithms for strong coupling procedures. *Computer Methods in Applied Mechanics and Engineering*, 195:2028–2049, 2006.
44. Hermann G. Matthies and Jan Steindorf. Partitioned strong coupling algorithms for fluid-structure interaction. *Computers and Structures*, 81:805–812, 2003.
45. M. Mehl, M. Brenk, H. J. Bungartz, K. Daubner, I.L. Muntean, and T. Neckel. An Eulerian approach for partitioned fluid-structure simulations on Cartesian grids. *Computational Mechanics*, 43(1):115–124, 2008.
46. Daniel P. Mok, Wolfgang A. Wall, and Ekkehard Ramm. Accelerated iterative substructuring schemes for instationnary fluid-structure interaction. In *First MIT Conference Computational Fluid and Solid Mechanics*, pages 1325–1328. Elsevier, 2001.
47. J. T. Oden, T. Belytschko, I. Babuska, and T. J. R. Hughes. Research directions in computational mechanics. *Computer Methods in Applied Mechanics and Engineering*, 192(7-8):913–922, 2003.
48. OpenCFD LTD. Openfoam home page, 2000–2009. http://www.opencfd.co.uk/openfoam.
49. Djordje Perić, Wulf G. Dettmer, and P. H. Saksono. Modelling fluid-induced structural vibrations: reducing the structural risk for stormywinds. In Adnan Ibrahimbegovic, editor, *NATO Advanced Research Workshop*, ARW 981641, pages 239–268, Opatija, Croatia, 2006.

50. Serge Piperno and Charbel Farhat. Partitioned procedures for the transient solution of coupled aeroelastic problems–Part II: energy transfer analysis and three-dimensional applications. *Computer Methods in Applied Mechanics and Engineering*, 190:3147–3170, 2001.
51. Anatol Roshko. *Of the Development of Turbulent Wakes from Vortex Streets*. Ph.D. Thesis, California Institute of Technology, Pasadena, California, 1952.
52. Michael R. Ross, Michael A. Sprague, Carlos A. Felippa, and K. C. Park. Treatment of acoustic fluid-structure interaction by localized Lagrange multipliers and comparison to alternative interface-coupling methods. *Computer Methods in Applied Mechanics and Engineering*, 198(9-12):986–1005, 2009.
53. M Schäfer and Stefan Turek. Benchmark computations of laminar flow around a cylinder. *Notes on numerical fluid mechanics*, 52:547–566, 1996.
54. Kenji Takizawa, Creighton Moorman, Samuel Wright, Jason Christopher, and Tayfun Tezduyar. Wall shear stress calculations in spacetime finite element computation of arterial fluidstructure interactions. *Computational Mechanics*, 46(1):31–41, 2010.
55. Tayfun Tezduyar, Kenji Takizawa, Creighton Moorman, Samuel Wright, and Jason Christopher. Multi-scale sequentially-coupled arterial FSI technique. *Computational Mechanics*, 46(1):17–29, 2010.
56. T.E. Tezduyar, S. Sathe, R. Keedy, and K. Stein. Space–time finite element techniques for computation of fluid–structure interactions. *Computer Methods in Applied Mechanics and Engineering*, 195(17-18):2002–2027, 2006.
57. T.E. Tezduyar, S. Sathe, J. Pausewang, M. Schwaab, J. Christopher, and J. Crabtree. Interface projection techniques for fluid–structure interaction modeling with moving-mesh methods. *Computational Mechanics*, 43(1):39–49, 2008.
58. S. Turek and J. Hron. Proposal for numerical benchmarking of fluid-structure interaction between an elastic object and laminar incompressible flow. *Lecture Notes in Computational Science and Engineering*, 53:371, 2006.
59. Wolfgang A. Wall, Daniel P. Mok, and Ekkehard Ramm. Partitioned analysis approach of the transient coupled response of viscous fluids and flexible structures. In *Solids, structures and coupled problems in engineering, proceedings of the European Conference on Computational Mechanics*, 1999.
60. Wolfgang. A. Wall and Ekkehard Ramm. Fluid-structure interaction based upon a stabilized (ALE) finite element method. Sonderforschungsbereich 404, Institut für Baustatik und Baudynamik, Germany, 1998.
61. Hongwu Wang and Ted Belytschko. Fluid-structure interaction by the discontinuous-Galerkin method for large deformations. *International Journal for Numerical Methods in Engineering*, 77(1):30–49, 2009.
62. Olgierd C. Zienkiewicz and Robert L. Taylor. *The Finite Element Method, Solid Mechanics*, volume 2. Butterworth Heinemann, Oxford, 5th edition, 2001.
63. Olgierd C. Zienkiewicz and Robert L. Taylor. *The Finite Element Method, The Basis*, volume 1. Butterworth Heinemann, Oxford, 5th edition, 2001.